**LA-UR-04-7014**

# APPLICATION GUIDE TO TOMOGRAPHIC GAMMA SCANNING OF URANIUM AND PLUTONIUM

J STEVEN HANSEN

SAFEGUARDS SCIENCE AND TECHNLOGY
NUCLEAR NONPROLIFERATION DIVISION
LOS ALAMOS NATIONAL LABORATORY

Supported by the U.S. Department of Energy
National Nuclear Security Administration
Office of Policy Integration and Technical Support (SO-13).

# TABLE OF CONTENTS

ACKNOWLEDGEMENTS

ABSTRACT....4

TGS GLOSSARY OF TERMS....5

INTRODUCTION....8

I. MEASUREMENT PRINCIPLES
- A. General Concepts....9
- B. Understanding Tomographic Image Reconstruction....14
- C. Defining the Geometry....19
- D. Attenuation and Emission Maps....21
- E. Detector Response Function....22

II. TGS DESIGN CONSIDERATION
- A. Transmission Source Assembly....25
- B. Detector Assembly....25
- C. Sample Positioning System....26
- D. Data Acquisition System....26
- E. Data Analysis Module....26
- F. Isotopic Composition....27

III. Operational Consider ions
- A. Calibration Procedure....27
- B. Typical Operational Steps....29
- C. Measurement Control Considerations....30

IV. PERFORMANCE EVALUATION IN BLIND TESTS AND ACTUAL FACILITY MEASUREMENTS
- A. Performance Demonstration Program (PDP)....32
- B. RFETS Pyrochemical Salts....45
- C. Uranium Applications....27

V. LUMP CORRECTION TECHNIQUE
- A. Plutonium Lump Detection and Correction Technique……49
- B. Standard Pu Lump Correction Doesn't Work For Uranium....50
- C. Proposal Technique For Uranium Lump Correction....51

VI. COMMERCIALLY AVAILABLE SYSTEMS....54

VII. REFERENCES....55

**ACKNOWLEDGEMENTS:**

The author is grateful the for the detailed technical reviews and editing assistance provided by Robert Beam of INL and Doug Reilly and Norbert Ensslin of Los Alamos National Laboratory. The superb breakthrough R&D efforts on the part of Robert Estep, Tom Prettyman, David Mercer, Stephen Betts, Chris Horley and John Lestone provided the bulk of the technical content for the present guide. Tim Elmont and Karen deAguero provide valuable input for the Glossary and the Operational Procedures sections.

# TOMOGRAPHIC GAMMA-RAY SCANNING OF URANIUM AND PLUTONIUM

## Abstract

This application guide was created to provide the user of the Tomographic Gamma Scanning (TGS) technology with a single comprehensive reference to the developmental aspects, underlying principles, and performance characteristics of modern TGS systems. The Department of Energy, National Nuclear Security Administration, Office of Policy Integration and Technical Support (SO-13) sponsored this project. For the new student of TGS, a glossary of specialized terms common to the field immediately follows this abstract. The glossary is followed by an introductory section giving a general history and a description of the material found in the remaining sections of the guide. The section on measurement principles begins with an illustrative description of the origin of the technology and its relationship to standard x-ray radiography. A sample problem leads the reader through steps designed to convey a conceptual understanding of the mathematical techniques used to reconstruct 3-dimensional images from the measured transmissions and emissions. Other factors such as detector response mapping, the relationship between the moving and stationary coordinate systems, and the determination of the isotopic abundance of the nuclear material constituents are described and references provided to allow a more detailed study. Important design factors are considered by studying each of the hardware modules and their associated design criteria. System calibration, operational steps and measurement control are important practical considerations and are described in some detail. Actual operational procedures as practiced in the production workplace are also provided. To allow an appreciation for the breadth of application along with the limitations inherent in the technique the results from the entire set of Performance Demonstration Program (PDP) tests are given. These blind tests combined with the results from extensive production plant operational results give the reader data from which to judge the applicability of TGS to their own plant applications. The specific application of TGS to the large inventory of uranium materials in the complex has not been exploited to the extent that plutonium material has been to date. A relative comparison of the sensitivity of the methodology is made between uranium and plutonium to point out that, in general, uranium is as amenable to TGS application as plutonium. A critical requirement for a broad based application of TGS is the ability to recognize the presence of macroscopic lumps of heavy metal and to make the appropriate corrections for self-attenuation. The plutonium lump correction is reviewed and a new method for uranium lump correction is introduced and described. The guide concludes with a list of current systems in operation, commercial availability and a comprehensive set of references.

## TGS GLOSSARY OF TERMS

**ART – Algebraic Reconstruction Technique** – A mathematical technique used to reconstruct tomographic images from attenuation data.

**Attenuation** - The propensity of high Z materials to reduce the gamma signal. Attenuation can be caused by the matrix, container packaging, or by the nuclear materials which give rise to the gamma emissions.

**CAT Scan** – Computer Aided Tomography scan using x-rays developed during the 1970's leading to the Nobel Prize for Medicine in 1979.

**Emission Tomographic Map** – A 3-dimensional graph of the distribution of nuclear materials determined from the intensity of gamma rays emitted from each voxel. The emission information must be corrected for absorption using the transmission map to determine the mass for the isotopes of interest.

**Heterogeneity** – Heterogeneity as it relates to NDA addresses both non-uniform distribution of the nuclear constituents within the matrix as well as variations in density and atomic number of the matrix containing the nuclear materials.

**Lump Correction** – A mathematical technique using differential attenuation of gamma rays from the same isotope in the determination of the correction associated with self-absorption of gamma–rays by the nuclear material. For all nuclear materials, other than those consisting of well-dispersed particles of microscopic size, the self-attenuation must be corrected for or an underestimation (negative bias) will result.

**Mashing** – Collapsing the raw data set is to improve the statistical quality of transmission measurements through dense regions of the target item.

**Monte Carlo Simulations** – Use of a computer code such as MCNP that has been developed to model particle or energy transport and probability of interaction within a system. The technique is often used as an effective means of conducting experiments computationally by modeling all aspects of the experiment that influence the movement of nuclear particles of varying type and energy.

**Opacity** – Opacity refers to the product of mass density times mass attenuation coefficient times material thickness. The quantity is unitless.

**PDP – Performance Demonstration Program** – A series of blind tests with standard matrix waste packages (drums or crates) are performed where standards are placed within the waste matrix and reported. Statistical tests are performed to assure the measurement platform lies within the accepted range for both precision and accuracy. Participation in this program is a requirement for facilities sending waste to WIPP.

**Pulse Height Spectrum** – A spectrum in which the voltage amplitude of a particular pulse is directly proportional to the energy of the particle creating the event in a detector leading to the pulse. For TGS a gamma spectrum of the nuclear isotopes of interest are rendered from the pulse height spectrum by a multi-channel pulse height analyzer. The latter may be either a standalone module or a software package within the computer data acquisition system.

**Projection** – The set of raysums acquired for a fixed rotation angle. This is roughly equivalent to a single radiograph of an object.

**Radiograph** – An image whose shading, from light to dark gray, represents the variations in the opacity of the object under study for a specific beam and sample orientation.

**Raysum** – The line integral of computerized tomography representing the opacity of a samplefor a specific beam sample orientation.

**Reconstruction** – Three-dimensional rendering of the distribution of attenuating materials or nuclear materials within a sample. The map of these distributions is reconstructed from the gammas observed from the sample for a large set of angular and dimensional coordinates.

**Segmented Gamma Scanner (SGS)** – The forerunner to Tomographic Gamma Scanner (TGS). An instrument that uses a horizontal collimator to assay slices of a sample

**Sinogram** – The image obtained through translation and rotation tomography of the target object.

**Tomography** - A method of producing a 3-dimensional image of an item by recording the differences in the effects on the transmission or emission of energy from or through the item.

**Transmission Correction** – By using a transmission source such as $^{75}$Se, the gamma-ray transmission can be measured accurately at several energies. By interpolating the transmission data, spatial maps of the attenuation coefficient can be obtained at any necessary energy. This information provides the matrix density allowing absorption correction for the determination of mass of the selected isotope.

**Transmission Tomography** – Tomography using an external emission source (for example $^{75}$Se). This information is important for determining the matrix densities of items. The transmission information is coupled with the emission tomography in determining the mass for the isotopes of interest.

**TRU Waste** – Transuranic Waste as defined by WIPP is waste containing radioactive constituents with an atomic number greater than 92, a half-life greater than 20 years and concentrations exceeding 100 nano-curies per gram of waste.

**Voxel** – Volume element or three-dimensional pixel used to define the location of the materials within the sample.

**WIPP** – The Waste Isolation Pilot Plant located in Carlsbad New Mexico, is an underground storage facility for nuclear waste operated by the Department of Energy.

# I. INTRODUCTION

The purpose of this guide is to provide users and potential users of the TGS technology a comprehensive reference document of the developmental aspects, underlying principles and performance characteristics of modern TGS systems. TGS was developed to measure residues containing special nuclear material and transuranic waste. Because a wide range of arbitrarily distributed isotopes must be quantified and the composition and distribution of matrix materials are generally unknown, these materials are extremely difficult to assay. TGS can be used to assay the bulk of this material, meeting both safeguards and performance requirements for nuclear material accountability and disposal at WIPP. The versatility of the technique is intended to reduce the cost and to greatly increase throughput of measurement operations.

TGS addresses two significant problems faced by the U.S. government: (1) timely closure and decommissioning of former nuclear weapons production facilities such as Rocky Flats; (2) disposal of radioactive waste produced by defense programs. Both of these problems have high public visibility and the Department of Energy has given their resolution high priority. The commercialization of TGS has enabled rapid and cost effective implementation of the technology at Rocky Flats. Because TGS can meet both safeguards and WIPP performance requirements with high throughput, implementation of TGS at Rocky Flats is supporting the site's mission of closure by 2006.

Development of the Tomographic Gamma-ray Scanning (TGS) technology began in the early 1990's (Refs. 1-4) in response to an increasing demand to assay a class of materials that were difficult or impossible to assay quickly and accurately with existing NDA techniques. The problem materials exhibited arbitrary distributions of nuclear material in a matrix of extreme heterogeneity in both density and composition. Techniques such as Segmented Gamma Scanning (SGS), which analyses emissions from the volume average of (imaginary) right circular cylindrical discs, or far-field gamma assay, which volume averages over the entire volume, often led to large errors and, given the difficulty of preparing representative standards, error estimates for any arbitrary samples were not reliable. Note that the difference between TGS and the older segmented gamma-ray scanner (SGS) is the addition of a translation axis that allows the detector to view the sample along all possible lines that pass through it rather than just through the radial centerline as in the SGS technology.

What was needed was a technique capable of viewing the sample as a composite of small volumes combined with a means of estimating the mass of the target isotopes within each small volume. Combining the principles of tomography with the power of high-resolution gamma-ray spectroscopy, the TGS technique was conceptualized and within a decade the TGS technique developed into one of the most robust, versatile NDA methods used in safeguards and nuclear waste measurements across the DOE complex.

Section II captures some of the development history of TGS and the underlying principles and presents a set of idealized image reconstruction problems to provide the reader with a good conceptual feel for the general mathematical approach underlying tomographic image

reconstruction. Section III provides a description of the hardware modules making up a typical TGS instrument. Where appropriate we try to provide helpful design criteria and guidance for systems to be used in production applications. The important practical aspects of TGS operation are covered in Section IV. To assist the reader in assessing the applicability of TGS to a particular class of materials, a section on its performance follows (Section IV).

The Performance Demonstration Program (PDP), sponsored by the Waste Isolation Pilot Plant (WIPP) in Carlsbad, NM, is a series of blind tests with standard waste drums designed to simulate typical materials that are destined to be shipped to WIPP for burial. All of the accepted NDA techniques for measurements of such materials were represented in the tests and the results provide an excellent starting point for the reader responsible for selecting the correct instruments for a particular task. In Section IV two real-life examples are given that illustrate the cost-benefit of TGS for certain classes of materials for which other NDA techniques are not well suited. The first example involves plutonium laden electro-refining salt residues at the Rocky Flats Environmental Technology Site (RFETS) in Golden, CO, and the second describes its application to a large inventory of 208-L (55-gal.) drums containing uranium contaminated materials. These examples illustrate that the high throughput and low bias of the TGS technique demonstrated in the PDP can carry over to the production environment when appropriate controls are applied and systems are properly designed. The principal limitation of the TGS for the assay of uranium and plutonium arises from the propensity for high-Z materials to strongly attenuate their own gamma rays. The extreme example of this problem is the self-attenuation of gamma rays in lumps of uranium (Z = 92) and plutonium (Z = 94). In materials that may contain these elements in non-microscopic sizes, a method for recognizing these conditions must exist and appropriate corrections must be applied to eliminate biases. Section VI is devoted to the subject of lump corrections, because of importance for the broader class of materials that may contain macroscopic lumps of SNM such as are found in many nuclear facilities. The TGS technology is now quite mature and available commercially and Section VII describes some designs available from commercial vendors.

## II. MEASUREMENTS PRINCIPLES

### A. General Concepts

In 1895, at the young age of 50, William Conrad Roentgen (1845-1923), working with a cathode ray tube (CRT), discovered quite by accident that some fluorescent crystals across the room gave off a green glow when the machine was on - even when the CRT was shrouded with a black cloth impenetrable by light. Such was the discovery of ionizing radiation that Roentgen named x-rays. Roentgen quickly followed his discovery by becoming the world's first radiologist, exposing films with various objects, including his wife's hand (Figure 1), placed between the CRT and the film. Within a year, battle surgeons were using x-rays to locate bullets in wounded soldiers and Henri Becquerel had discovered natural radioactivity. The atomic age was born.

Radiographs such as that of Mrs. Roentgen's hand have been critical tools in the fields of medical and industrial diagnostics. The radiographic technique consists of focusing a broad parallel beam of penetrating radiation upon a sample of interest and recording the effects of the

unabsorbed portion of the beam upon the radiographic film. The picture or image provided by the film is really just a representation of the opacity of the sample, which varies dependant

***Fig. 1.*** *Radiograph of Mrs. Roentgen's hand.*

upon the density, thickness and atomic number (Z) of the sample. In the case of a biological sample such as Mrs. Roentgen's hand, the calcium in the bones is of higher atomic number ($Z$=22) and density than the surrounding flesh and preferentially attenuates the beam and correspondingly underexposes the film relative to the surrounding areas where bone is not present. Opacity differences as small as a few percent can be discerned under ideal conditions and high quality images can be obtained which are an invaluable diagnostic for the medical and the industrial community. X- ray radiography works perfectly well to image materials that do not completely attenuate the beam, that have differences in attenuation (opacity) due to internal structure that the radiographer wishes to study, and that can be oriented perpendicular to the x-ray beam. Consider the problem of producing the radiograph of Mrs. Roentgen's hand when the hand is rotated by $90^{o}$ relative to the x-ray beam, i.e. thumb toward the CRT and little finger toward film. The bones of the fingers would all then coalesce in the image plane and such a radiograph would be virtually useless for producing the desired detailed imaging of each finger. This is the very problem that tomography was designed to solve – How to render an image of an object in three dimensions so that any arbitrary plane of interest can be displayed when the source and detector or film can not be placed at right angles to the plane of interest? The technique of tomography requires extensive manipulations of large data sets and, therefore, awaited the development of computers. As a benchmark, during the period circa 2000, some analyses could take many minutes to be completed with the speed and data handling capabilities of that time. (Processor speeds at that time were roughly 500 MHz) In the future analyses can be

expected to be effectively instantaneous, thereby allowing real time assessment of the quality of the results and the possibility of remeasurement before sample unloading.

Consider Figure 2, which compares the radiographic method with the tomographic method using a pair of concentric metal washers as the sample. The point of this comparison is to provide a simple conceptual feel for the ability to produce an image in tomography similar to the image produced in normal radiography. Under normal circumstances with a thin sample such as depicted in the figure, standard radiography would be the preferred method, but in the case of samples so thick to not permit a standard x-ray, tomography provides an alternative means for "seeing inside the object"

In figure 2, the plane of interest, xy, is parallel to the surface of the page and taking a radiograph of the washers with the orientation of beam, sample and film as depicted would be expected to produce a good image of the washers as depicted in the figure. Using tomography, one can reproduce a similar image as depicted in the figure immediately below. The method illustrated here chooses three angles of incidence relative to the two washers (horizontal, vertical and diagonal) and then moves the object (or source and detector) in small steps from one side of the large washer to the other side. In our example, for each of the three angles approximately a dozen measurements or data grabs are made in scanning from one side to the next. At each measurement point the count rate from the radiation source is recorded by the radiation detector and varies with the inverse of the opacity of the sample along that line of incidence. The resulting count rate is often referred to as a projection or raysum.

Figure 3 gives a simple example defining a projection or ray-sum. In this example the sample has been divided up into 10 rows and 11 columns and the $5^{th}$ row is currently being interrogated with the radiation source and the count rate is inversely proportional to the opacity as defined in the equation at the bottom of the figure. It is clear that the total opacity is simply the sum of the opacities of the different cells making up the $5^{th}$ row and that the individual opacities are a product of the linear attenuation coefficient and the thickness ($\Delta X$) of the cell.

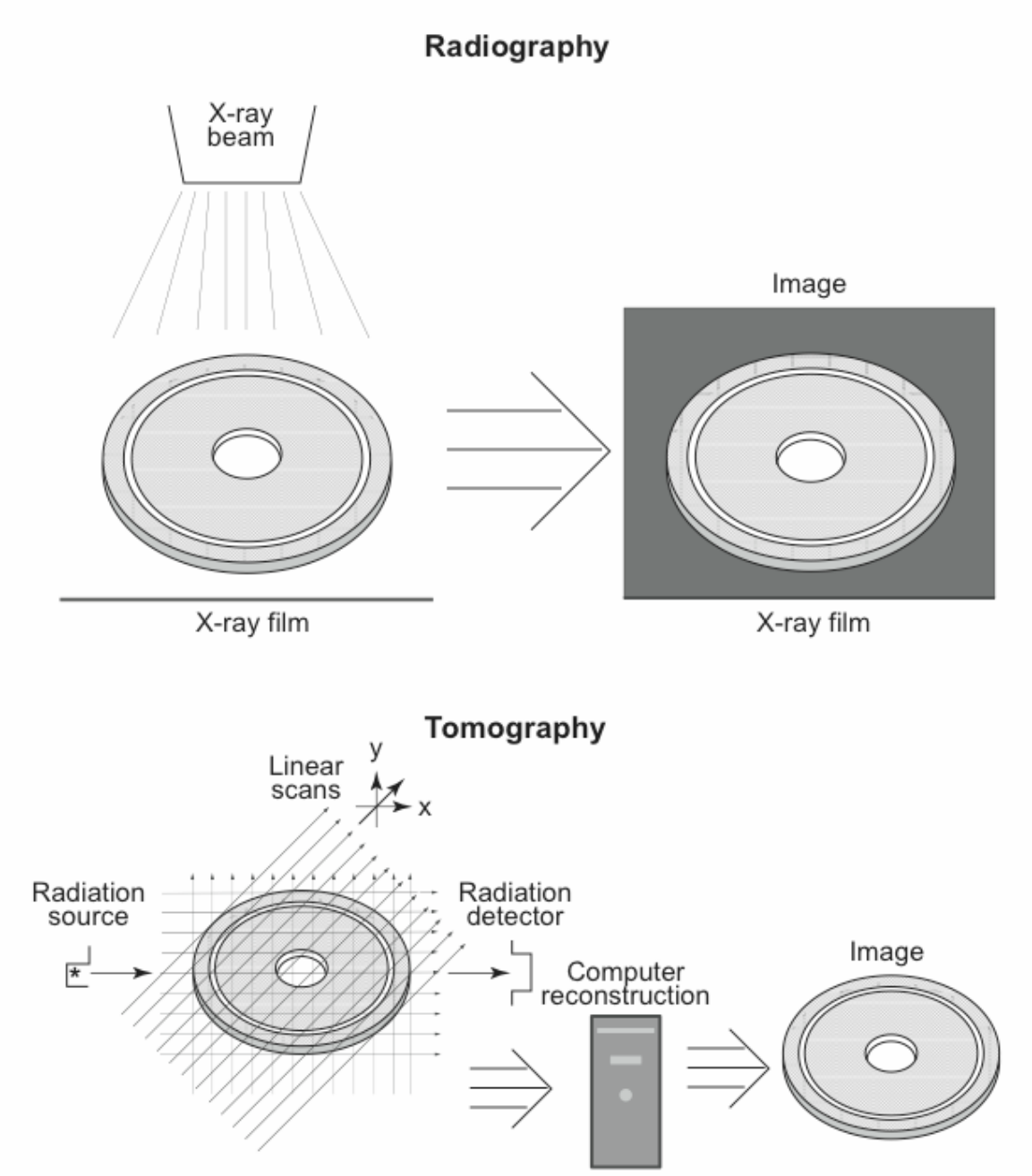


***Fig. 2.*** *Radiography and Tomography.*

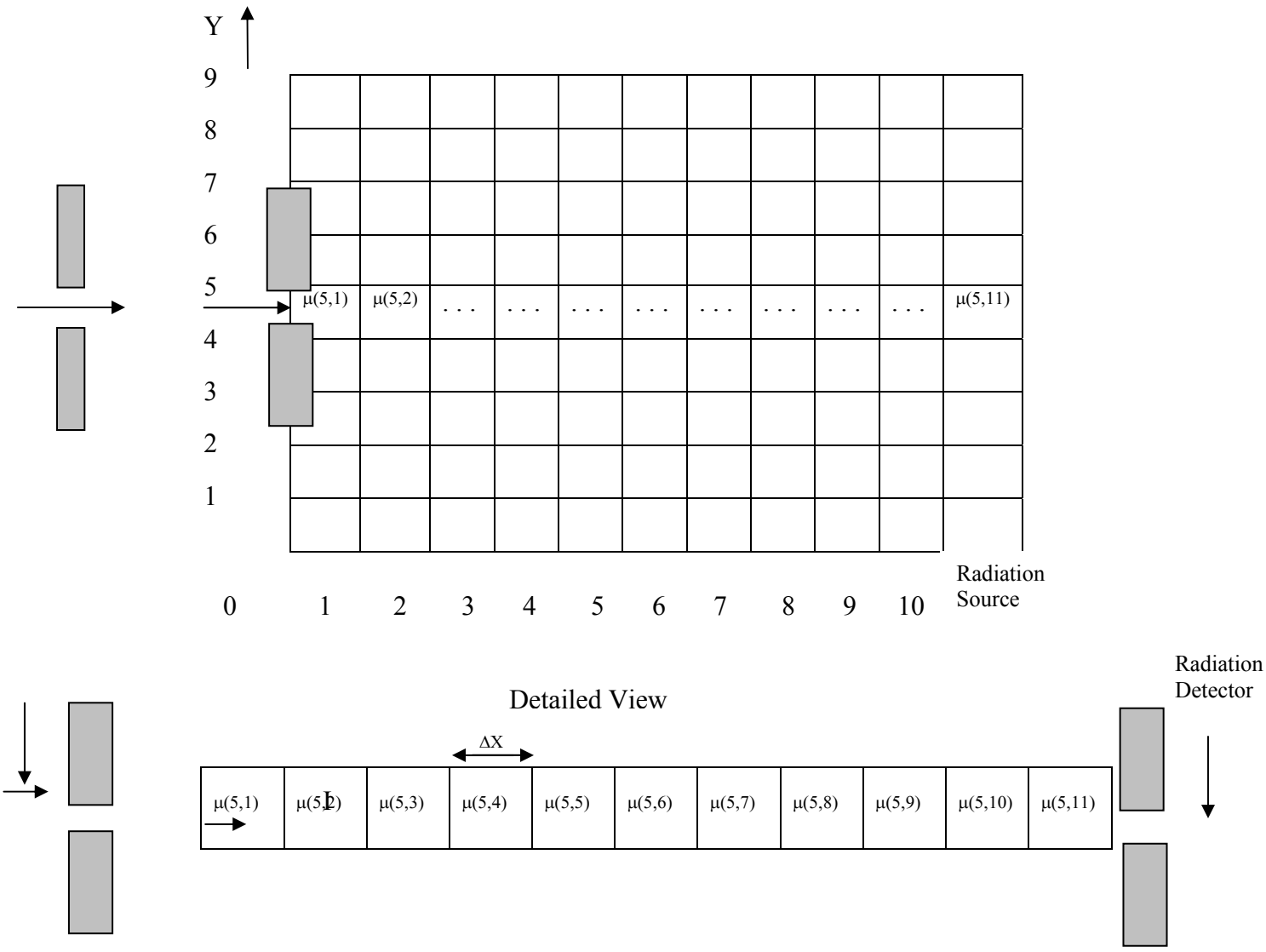


$$I = I_O\, e^{-\left[\mu(5,1)\Delta X_1 + \mu(5,2)\Delta X_1 \ \ldots\ldots\ldots\ldots \mu(5,11)\Delta X_{11}\right]}$$
$$= I_o\, e^{-\left[\mu(5,1) + \mu(5,2) \ldots\ldots\ldots\ldots \mu(5,11)\right]\Delta X}$$

where I and $I_0$ represent the intensity of the transmitted and incident beam and the quantities in brackets represent the linear attenuation coefficients of the various cells.

when $\Delta X_1 = \Delta X_2 = \ldots\ldots\ldots\ldots\ldots \Delta X_n = \Delta X$

The expression below represents the opacity of the 5th row.

$$\left[\mu(5,1) + \mu(5,2) \ldots\ldots\ldots\ldots\ldots \mu(5,11)\right]\Delta X$$

***Fig. 3.*** *Projections or ray-sums are opacity measurements.*

## B. Understanding Tomographic Image Reconstruction

Although the detailed algorithms and explicit mathematics associated with tomographic image reconstruction from raysums can be complex [5,6] our purpose is to understand the underlying concepts through the study of a set of simple idealized tomographic reconstructions. To this end we use a very straightforward iterative technique to solve for the opacities of rectangular cells that geometrically define our objects and begin with the 1x1 matrix to demonstrate the rules for this technique. We then successfully apply the same rules to more complex matrices (2x2 and 3x3) and using mathematical inference we assume the technique will work for any matrix of arbitrary dimension.

We begin with Figure 4a the simplest case of tomography, the 1x1 matrix and for the purpose of demonstrating the method we have quite arbitrarily assigned it an opacity of 5. As a general rule the initial guess is not particularly important, at worse if particularly bad leading to one more iteration in more complex problems. As in Figure 2, we will restrict our data to horizontal, vertical and diagonal projections, whereas in real tomography other projection angles might be used to provide a larger data set. Obviously the horizontal, vertical and diagonal projections will each give a total opacity of 5. Having acquired this data we will blindly follow the rules for image reconstruction given below and compare our estimates with the actual opacity (5) of the cell. This technique we use is a common one called the Algebraic Reconstruction Technique (Ref. 5).

Rules for the Algebraic Reconstruction Technique (ART)

1. Sum and record the actual projections ($P^0$) for all angles.
2. Make an initial guess at the opacity ($O^i$) for each of the cells.
3. Calculate the projection for one of the angles for all cells using the latest estimate for the opacities. NOTE: The latest estimate in the case of the first estimate is a guess.
4. Compute each new iteration from the results of the last with the following equation where N is the number of cells in the particular projection under analysis.

$$\mathbf{O^{i+1} = O^i + (P^0 - P^i)/N}$$

5. Compare final estimates of the cell opacities once all projections have been applied.

Referring to the 1x1 opacity matrix in Figure 4, our analysis begins with a guess for the initial opacity ($O^i$) of zero (0). Even with this poor guess this simple problem immediately converges to the correct result in the first iteration. This of course holds true regardless of the angle of incidence of the projection (horizontal, vertical or diagonal). In Figure 4b, within each cell, the $i^{th}$ opacity is given immediately above the calculated i+1 opacity with a dashed line separating the two values. In general, we have calculated estimates for the cells in the first column of each matrix. The reader may wish to verify our calculations for the remaining cells.

**1 x 1 Opacity Matrix Reconstruction Example**

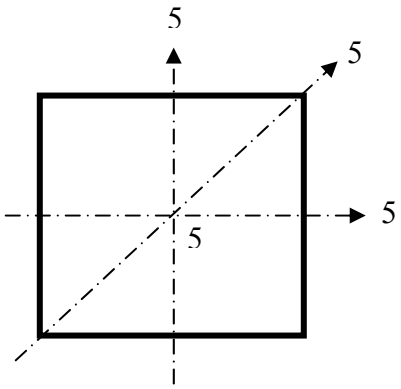


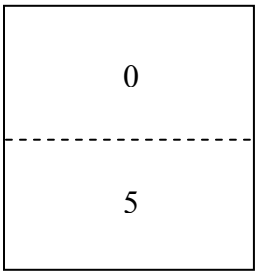


Guess

Estimate = E

For All Projections

$$E = 0 + \frac{[5-0]}{1} = 5$$

***Fig. 4a***

---

Having validated our technique for the 1x1 matrix, we now apply it to a 2x2 matrix. Note that after using the four projections for the horizontal and vertical angles of incidence, our estimates for the opacities have improved yet still are rather poor. This is in fact generally the case in tomography that the estimates improve with the number of projections and that exact solutions are rare. Only after applying the diagonal projections to our analysis technique do we find the technique provides a unique and correct solution, matching exactly the "unknown" opacities. In cases of matrices of larger dimension, even with simple well-defined geometries and cell opacities, generally unique solutions will not exist and final results will depend upon the number of projections and in some cases on the initial guess and the order in which the projections are taken in the analysis.

**2 x 2 Opacity Matrix Reconstruction Example**

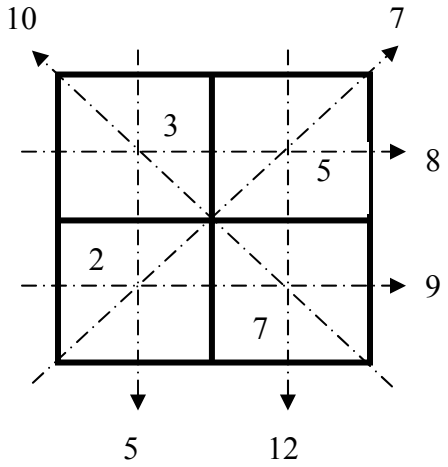


***Fig. 4b***

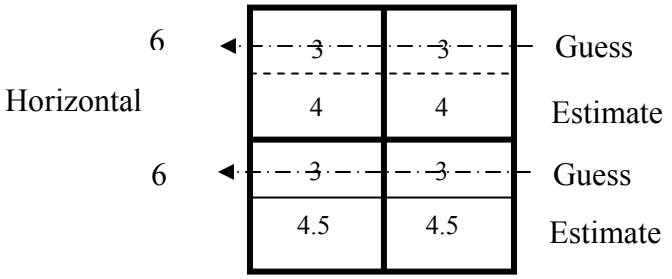


$$E = 3 + \frac{[8-6]}{2} = 4$$

$$E = 3 + \frac{[9-6]}{2} = 4.5$$

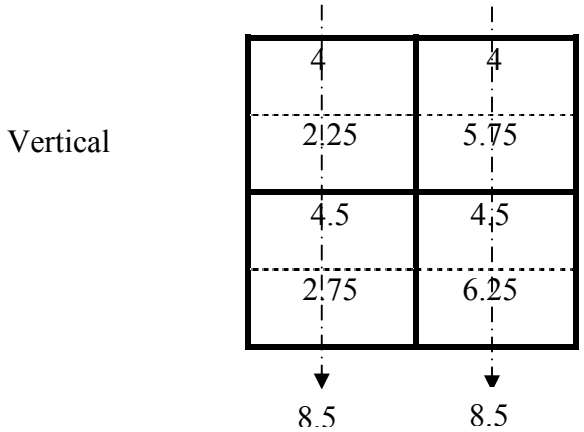


First Column Estimates

$$E = 2.25 + \frac{[10-8.5]}{2} = 3.0$$

$$E = 4.5 + \frac{[5-8.5]}{2} = 2.75$$

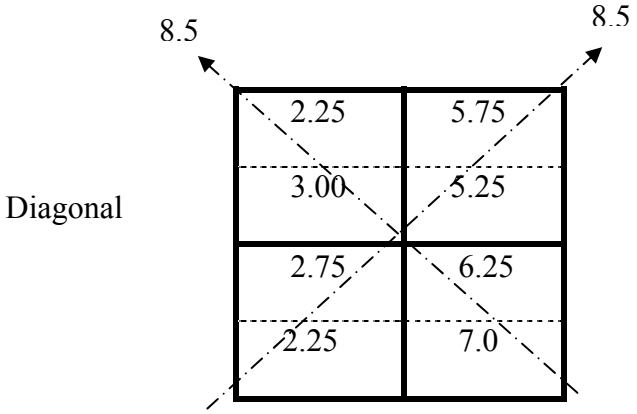


First Column Estimates

$$E = 2.25 + \frac{[10-8.5]}{2} = 3.0$$

$$E = 2.75 + \frac{[7-8.5]}{2} = 2.0$$

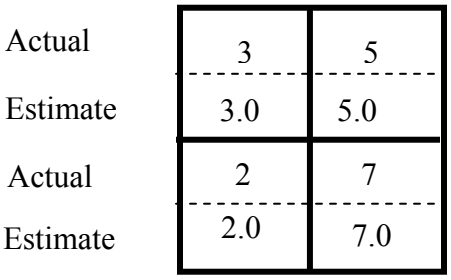


Comparison of Final Estimates with Actual Opacity.

***Fig. 4b** continued.*

The 3x3 matrix problem below illustrates the problems associated with too few projections. We have eliminated the actual calculations for all but the horizontal projections. Beginning with an initial guess of 5 for all cell opacities and proceeding from the horizontal incidence to vertical to left to right diagonal and then right to left diagonal the reader can verify our results at the bottom of Figure 4c. The problem of using too few projections is made clear by comparing the results of the analysis between the two analyses: the first in which we include all of the corner projections and the second where we do not include the corner projections, Figure 4c. The results when the corner projections are not included are very poor and in the case of the upper right corner cell the estimate is in excess of three times the actual opacity.

**3 x 3 Opacity Matrix Reconstruction Example**

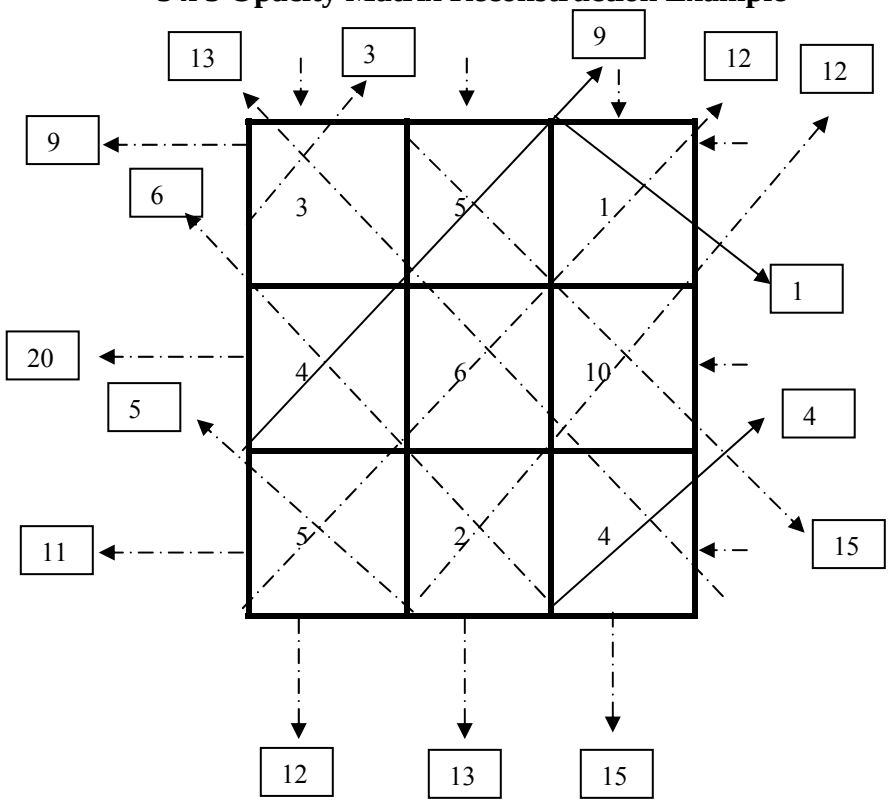


The above are the actual projections or ray-sums.

Preliminary guess and new estimates

Horizontal

| | | | |
|---|---|---|---|
| Guess | 5 | 5 | 5 |
| Estimate | 3 | 3 | 3 |
| Guess | 5 | 5 | 5 |
| Estimate | 6.67 | 6.67 | 6.67 |
| Guess | 5 | 5 | 5 |
| Estimate | 3.67 | 3.67 | 3.67 |

First Column Estimate

$$E = 5 + \frac{9-15}{3} = 3$$

$$E = 5 + \frac{20-15}{3} = 6.67$$

$$E = 5 + \frac{11-15}{3} = 3.67$$

| | | | |
|---|---|---|---|
| Guess | 3.0 | 5.0 | 1 |
| Estimate | 3.04 | 5.0 | 1 |
| Guess | 4.0 | 6.0 | 10.0 |
| Estimate | 4.0 | 6.06 | 10.0 |
| Guess | 5.0 | 2.0 | 4.0 |
| Estimate | 5.0 | 2.0 | 4.04 |

Final Estimates Compared to Actual Projections

***Fig. 4c*** *The 3 x 3 image reconstruction with Corner Projections*

| | | | |
|---|---|---|---|
| Guess | 3 | | 1 |
| Estimate | 2.59 | | 3.11 |
| Guess | | | |
| Estimate | | | |
| Guess | 3 | | 4.0 |
| Estimate | 2.78 | | 4.26 |

***Fig. 4c (cont.)*** *The 3 x 3 image reconstruction without Corner Projections*

So in conclusion, we have demonstrated that by using a simple iterative technique, three angles of incidence, and sufficient projections at each of the three angles that very good reconstructions are possible. Thus one might expect for example that by applying our technique to the problem of Figure 2, a reasonable image of the two washers could be produced. This technique provided the basis for Computer Aided Tomography (CAT) scan analysis developed during the 1970's (Refs. 6-9) and leading to the Nobel Prize for Medicine in 1979. Such techniques have undergone refinements but the underlying approach is similar to that applied to our simple problem. In the medical field such techniques currently provide high accuracy image reproductions at the sub-millimeter level. We have discussed the reproduction of thin slices using tomography assuming that the data is of high quality statistically. In TGS this normally is the case for transmission scans but rarely so for emission scans. In the latter case, many of the voxels are void, the angle of view is large and the full energy peak can be difficult to distinguish above the continuum. Under these conditions conventional methods of Least Squares or Algebraic Reconstruction Techniques may not produce satisfactory results. To deal with these cases TGS developers have applied and refined techniques related to the Maximum Likelihood Reconstruction Method[10], defining the data in statistical terms or Poisson variates. The technique executes an iterative approach until the distribution of materials provides the best

match or (Maximum Likelihood) to the statistical data. The reader is referred to References 11 - 18 for a description of the various innovative techniques that have been developed to adapt the aforementioned approach to the application of difficult materials found in the DOE complex.

## C. Defining the Geometry

Figure 5 is a schematic of a generic TGS showing the general relationship of the sample, the source, and the high-resolution germanium detector. For a typical one hour scan of a 208-L drum at each of 10 to 15 axial positions, the drum would rotate at approximately three revolutions per minute while translating in a horizontal direction at approximately 30 cm/min. In Figure 6, the two coordinate systems are shown which are used to uniquely define the motion of the drum. The graph indicates the individual measurement points as a function of the angle of rotation of the drum and the distance the drum has moved from the origin. In a typical scan, the drum would start with its outer edge grazed by the collimated beam from the $^{75}$Se attenuation source. It would then rotate at 3 rpm while translating to a position where the $^{75}$Se beam intersected the radial centerline of the drum. The direction of translation would then reverse and the drum would return to its initial position. The round trip would take approximately 2 minutes during which time approximately 150 separate data grabs would be acquired. The mathematics relating functions defined within these two coordinate systems were published first by Johann Radon in 1917 (Ref. 19) but went undiscovered through much of the early development of the tomography technique. The idea, nevertheless, is that by means of the Radon transformation a two-dimensional function (such as the opacity as a function of position in the x,y plane) can be inferred from the projections which are defined in terms of an angle of rotation, $\theta$, and translation of the object in a direction, s, relative to the stationary x,y coordinate system. The drum is then moved vertically ( or in the Z direction in standard Cartesian coordinates) approximately 5 cm and the scan is repeated. By stacking sections or slices one can reproduce a three-dimensional object through superposition. For those who are interested in formulations of a mathematical nature, they are referred to the original article by Radon.

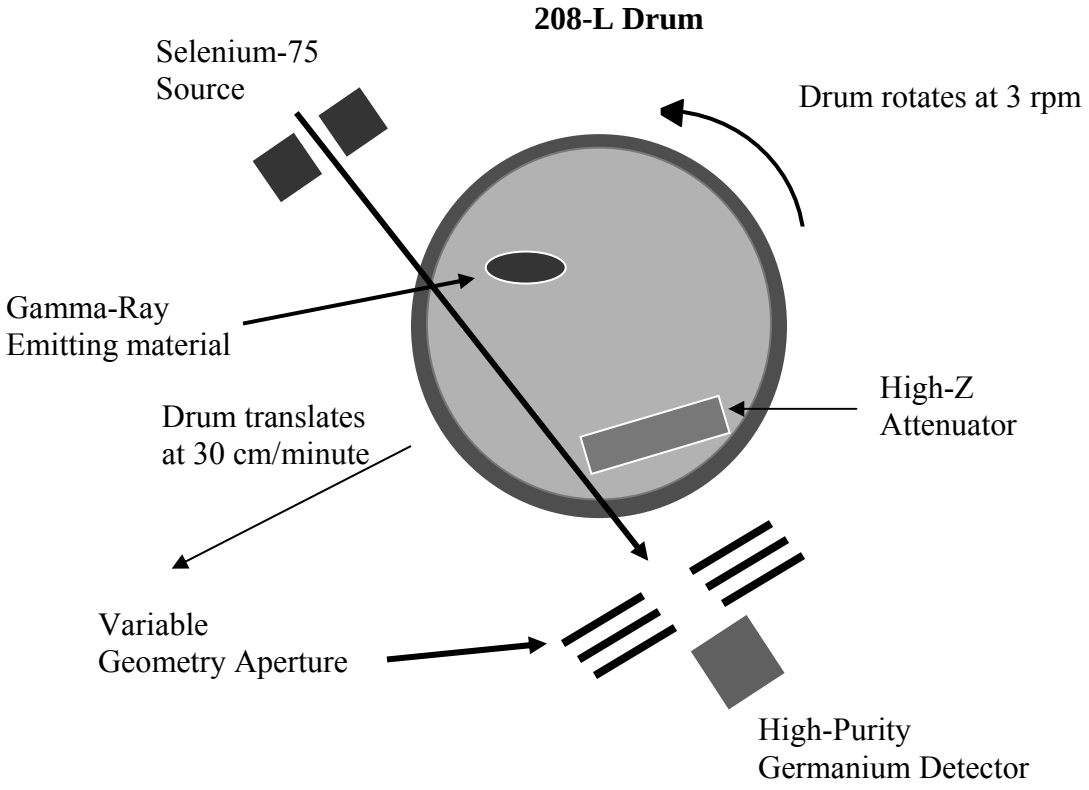


***Fig. 5.*** *The TGS configuration in concept.*

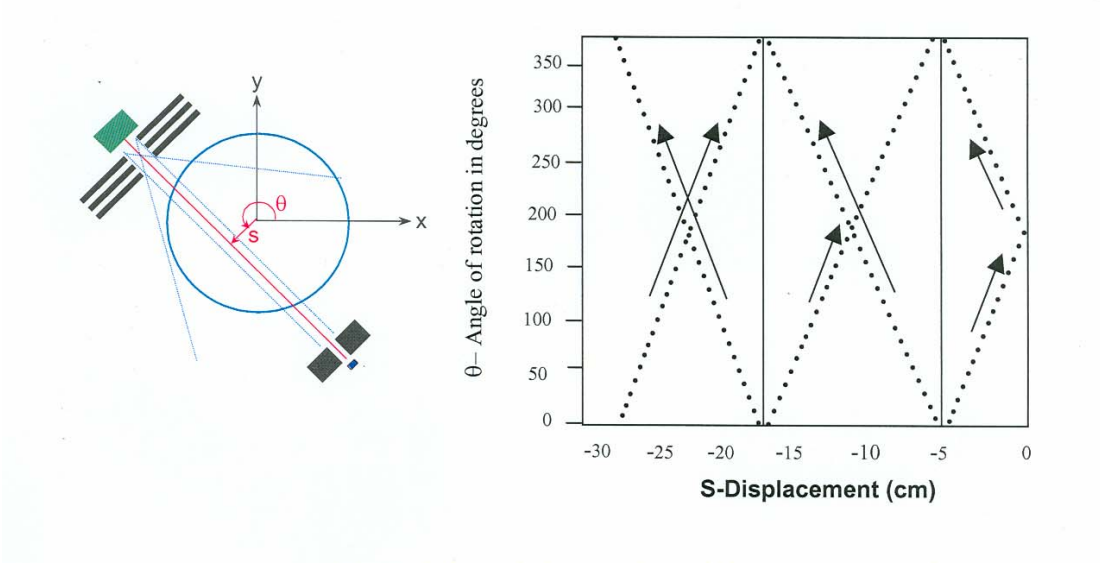


***Fig. 6.*** *The stationary and moving coordinate systems.*

## D. Attenuation and Emission Maps

The TGS method counts gamma rays emitted by plutonium or uranium in contiguous small volume elements distributed throughout the sample estimating the mass of SNM from the counting rate of certain characteristic gamma rays. The gamma rays are detected with a high-purity germanium (HPGe) detector and corrections are applied to the count rate for the attenuation by materials intervening between the small volume elements and the detector. The problem of nuclear material NDA with gamma-ray tomography is one of defining a three-dimensional image of a sample (say a 208-L drum) in terms of a set of three-dimensional "pixels" often termed voxels (volume + pixel) and assigning the appropriate mass of SNM and opacity to each voxel. In effect, the problem is reduced to conducting a gamma-ray assay for each voxel within a 208-L drum. For a 208-L drum divided into approximately 1500 voxels, this corresponds to breaking the problem into an assay of volumes that are roughly 5x5x5 $cm^3$. By suitable image reconstruction techniques, the result of a tomographic assay is to associate with each of these voxels a mass of SNM and opacity.

To estimate the contribution from a particular voxel to the count rate the gamma-rays emitted by the materials in the voxel are ray-traced to the detector and attenuation corrections are made by summing the opacities of the voxels through which the rays must pass. The image reconstruction of each voxel is involved since the voxels that lie between it and the detector vary as the drum rotates and translates and the germanium detector samples a large volume (many voxels) of the sample, see Figure 6. Nevertheless, by careful geometric definition of the fixed and stationary coordinate systems and the application of efficient reconstruction algorithms, high throughput, low bias, and adequate image reconstruction can be achieved. Having completed the analysis, each voxel is assigned a mass of a specific isotope and an opacity value. Combining the results for each voxel produces a map of the attenuation and another for the emission characteristics of the drum as a function of position (x,y) within the drum. Such maps are shown in Figure 7 for four drums (76 cm high x 61 cm diameter) of varying matrices and $^{235}U$ mass. The resolution is of the order of a voxel length, 5 cm, and the color red indicates the highest concentration of either matrix material or 235U. The attenuation map is to the left of the emission map for each of the four drums.

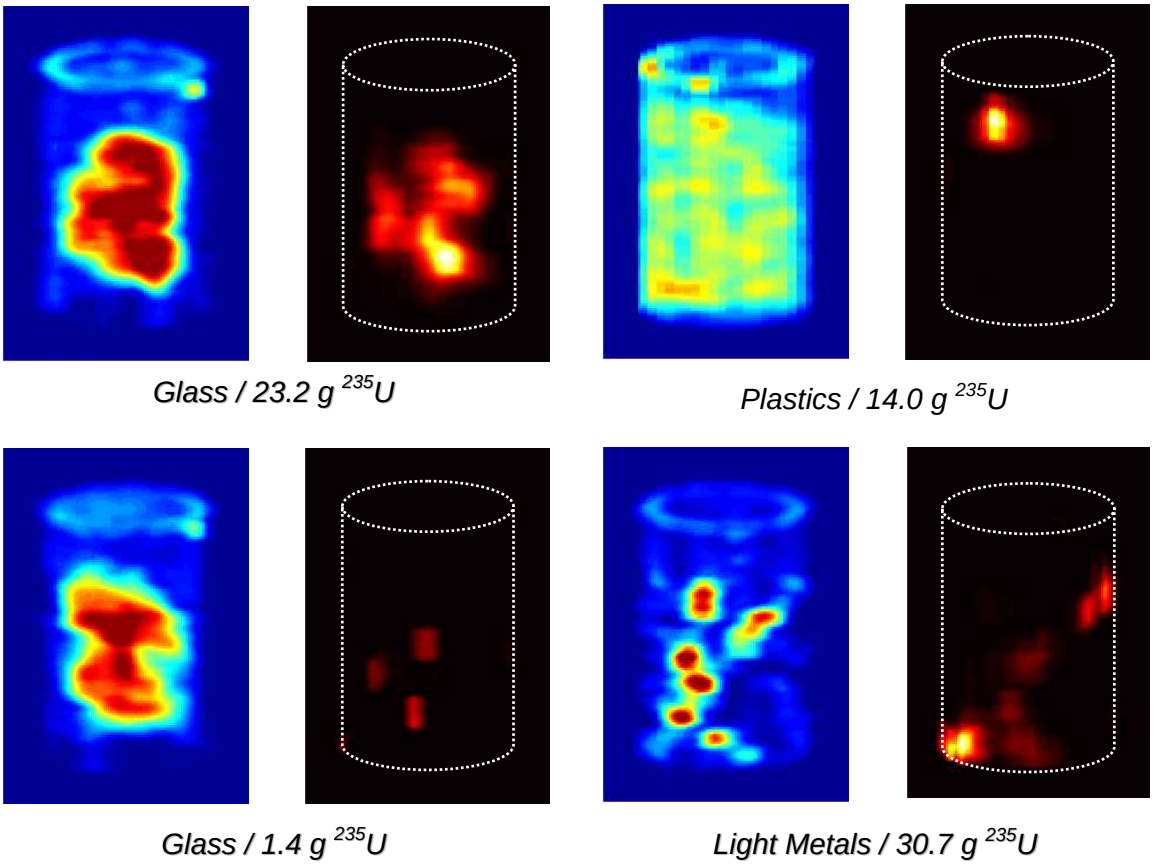


***Fig.7*** *Transmission and emission image reconstructions of 208 liter drums in varying matrices. The blue background is the attenuation map and the black is the emission map.*

## E. Detector Response Function

The foregoing sections describe some of the fundamental principles of tomography whose aim is to reconstruct images or produce maps similar to those in Figure 7. The images tend to be proportional to the measured count rates and to convert the measured count rates to estimates of isotope mass some critical steps must be carefully undertaken. These steps are best understood through consideration of the parameters within the assay equation below. The sought after mass is proportional to the number of atoms Ni and the count rate of gammas from the mass represented by that isotope is a function of the decay rate λ, branching ratio and the detection efficiency given by the last parameter in the equation.

$$C(E_i) = \lambda * N * BR(E_i) * \varepsilon(E_i)$$

The first two terms on the right side of the equation are the decay constant, $\lambda_i$ [$sec^{-1}$] and the number of atoms, $N$, of the isotope under observation. The product of these two terms produces the decay rate in disintegrations/second. The mass of the isotope (which is what we seek) is of course proportional to number of atoms of that isotope. *BR(E)* is the fraction of decays of the isotope which lead to the production of the gamma of energy E.

The last term in the equation, $\varepsilon\left(E\right)$ is called the absolute efficiency It is the **probability that an emitted gamma ray of energy E actually is counted in the full energy peak of the detector**. If we were dealing with a point source on the axis of the detector with no intervening materials the assay of the mass would be easy. Considering that these gammas are emitted from masses at varying distances, at angles oblique to the detector axis and through materials with widely varying attenuation properties, accurately predicting the last term for every mass element is non-trivial.

TGS breaks the problem of computing the absolute efficiency into two components - one associated with the sample and the other with the detector. The component associated with the sample obviously varies from sample to sample and is inferred from the results produced from the emission and transmission scans.

The component associated with the detector is the probability that an unshielded emission, from any arbitrary point within the container, actually yields a count in the full energy peak. The accuracy of the assay is no better than one's ability to accurately determine this probability for all points within the container.

Because this factor varies dramatically with distance, with angle due to the effects of the collimator and with the intrinsic efficiency of the detector for differing angles of incident photons, to attempt to experimentally map this space would be enormously time-consuming. As a substitute the experiment is conducted with Monte Carlo calculations, which model the geometry and the detector, and is normalized to experimental results at selected points.
To setup the model one of course must have all of the pertinent parameters very accurately known. Some of these can be measured quite accurately, e.g. the distance from container surface to collimator front face, collimator opening and depth. Others such as the actual dimensions of the active region of the detector must be approximated from the manufacturer's specification. In the end, of course, for the calculation to provide useful results all pertinent dimensions and material properties must be well characterized. The variations with distance and angle are handled reasonably well by the calculation but the actual intrinsic efficiency as a function of energy and angle of incidence is handled less well. Therefore, an iterative process is necessary which includes actual measurements, placing standards of well known emission rates at strategic points in the container and predicting their emission rates based on the most recent model. Provided that one has pre-established the optimum detector to container standoff, the optimum collimator opening, and the desired scan time, one could rather efficiently generate an accurate map after several such iterations

In the present case in order to optimize throughput, while maintaining the necessary precision, variations in the collimator size and, possibly container to collimator standoff, must each be investigated and from a bare minimum of such studies the best compromise must be inferred.

In medical tomography, high-resolution imaging is essential. In the application of tomography to the assay of radiological samples, such as 208-L drums of contaminated waste, throughput is the key issue and high throughput requires large apertures and large germanium detectors. As such, the view and efficiency of such detectors is great and varies for a particular point in space with the inverse of the distance from the detector and, to a lesser extent, to the degree that the point is off the detector axis. It is important to apply these corrections to the detection efficiency and, as a general rule, a detector response curve must be generated for each aperture setting. Figure 8 is the detector response function for an x-axis distance from the detector of 92 cm and a y axis distance varying from –40 cm to 40 cm. At roughly 30 cm, the effects of the tungsten collimator eclipse the source emissions and the count rate falls to zero. Curves such as Figure 8 are normally generated by applying computer models supported by experimental measurements.

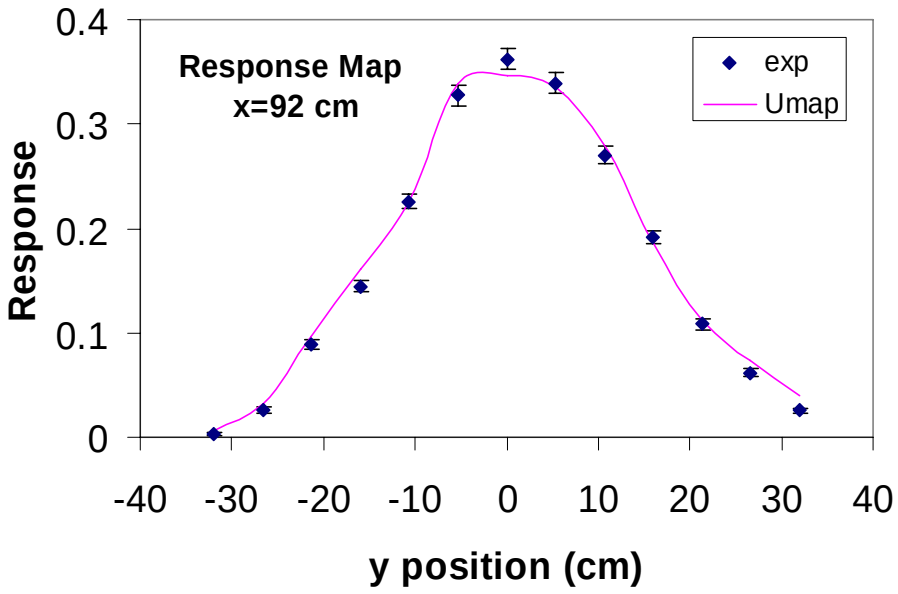


***Fig. 8.*** *Detector response map.*

## III. TGS DESIGN CONSIDERATIONS

The design details of TGS systems can vary depending upon the dimensions and weight of the samples to be measured, whether the principal use is in a production environment or in a research laboratory, and to some extent upon the acceptable precision and bias. Versatility, accuracy, and throughput come at a price, but all systems require certain functions or modules to perform. In this section, we will consider the TGS as comprised of these modules and point out some of the design considerations in their selection.

Figure 9 is an engineering drawing for a TGS system fielded from 1998 – 2003 at RFETS (Transportable TGS - TTGS) and the progenitor of the commercial models available through license agreements with Los Alamos National Laboratory. The TTGS was designed for versatility, accuracy, and high throughput in a production environment. In the next Section IV, the results from one of its major assay campaigns is described. It was designed to be very modular and it is well suited for the present discussion. The major modules are the Transmission Source Assembly, the Detector Assembly Module, the Sample Positioning System, the Data Acquisition System, and the Data Analysis Module. Each of these is discussed in turn.

## A. Transmission Source assembly

The transmission source is mounted in a tungsten shield on top of a 2.5-m steel tower. A high intensity (30 to 200-mCi) $^{75}$Se source is used to provide high throughput and penetration of dense samples (e.g. cement in 314-L overpacks). Using $^{75}$Se for the transmission source, gamma-ray transmission can be measured accurately at several energies near the important lines of $^{239}$Pu and $^{235}$U. By interpolating the transmission data, spatial maps of the attenuation coefficient can be accurately obtained at the gamma-ray energies of interest. The only drawback to the use of $^{75}$Se is its relatively short half-life (120 days) that requires sources to be replaced annually. A solenoid-driven tungsten shutter (5 cm thick) provides a tightly collimated beam (0.3-cm diameter) of gamma rays for transmission measurements when in the open position,. For this system, a low-power laser/silicon diode alignment system verifies the alignment of the source and detector. Such enhancements may be considered when systems are to be placed in a rugged production environment.

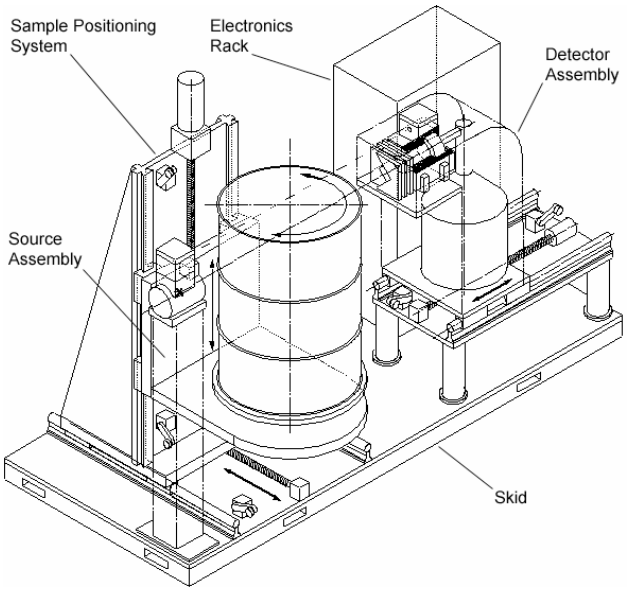


***Fig. 9.*** *RFETS transportable TGS outline drawing.*

## B. Detector Assembly

The detector assembly has an HPGe detector, a live-time source ($^{109}$Cd), a collimator, and shielding. The detector combines high efficiency (> 50%) with high resolution to permit gamma-

ray isotopic measurements from the composite spectrum from the emission scans. The opening of the collimator is adjustable by stepping motors from 1.25 cm to 6.4 cm to accommodate a large range of sample sizes. The detector assembly is auto-positioned depending on the sample size selected by the operator. These automated provisions add cost and are not necessary for a research environment or in a production environment in which supervisory oversight can be substituted for automation. For low Pu or U mass measurements in a production environment thick tungsten shields are necessary. The detector is adequately shielded by 10 cm of tungsten.

## C. Sample Positioning System

The sample positioning system has a three-axis precision stage driven by stepping motors that provided sample translation, rotation, and elevation relative to the source and detector. Note that the difference between TGS and the older segmented gamma-ray scanner (SGS) is the addition of a translation axis that allows the detector to view the sample along all possible lines that pass through it rather than just through the radial centerline as in the SGS technology. By stacking slices (axial scanning), the spatial distribution of material within the entire sample can be recovered and a three-dimensional mapping of the drum contents is possible. The RFETS system accommodates sample sizes ranging from 15 cm to 75 cm in diameter and up to 908 kg total weight. The largest samples were 303-L drums and the smallest were 2-L cans. In a typical transmission scan of a 208-L drum, the drum rotates at 3 rpm, makes 5 entire revolutions, and takes 150 data grabs of the entire spectrum for each axial layer. The total transmission scan of 16 layers takes 30 min, then the drum mounting stage and drum return to the initial position, the shutter is closed, and the scan protocol is repeated with a high degree of repeatability ($< 0.013$ cm total maximum repeatability error).

## D. Data Acquisition System

High throughput and accurate, unbiased results are the hallmark of a well-designed TGS system. Current data acquisition systems, if well specified, should not be the limiting factor. General requirements might include grabbing and storing 5000 measurements per hour with individual grab times of approximately 2/3 s. Each measurement is associated with a particular projection as depicted in Figure 6. Summing these measurements provides an average spectrum suitable for post-scan isotopic abundance determinations.

## E. Data Analysis Module

During the emission scan, the sample is scanned with the transmission source shuttered off and net counts are recorded for regions of interest (ROIs) about peaks corresponding to gamma rays emitted by the target isotope. For plutonium assays, ROIs are typically established for four well-resolved gamma rays: 129-, 203-, 345-, and 414-keV. Each of these gamma rays is used to develop an independent estimate of the distribution and mass of $^{239}$Pu within the sample. When large variations are observed for the different energy estimates, the presence of self-attenuating lumps is indicated and lump correction algorithms must be applied. (See Section VI.) As the sample rotates and translates relative to the detector, the net count rate varies. The magnitude of the net count rate depends on the distance from the gamma-ray source to the detector and the intervening attenuating material. Since the attenuation map is known for each gamma ray energy

of interest, the net count rate can be calculated for trial distributions of the emitting material. Reconstruction of this spatial distribution of emitting material is accomplished by adjusting the trial distribution until the estimated net counts match the measurements (Refs. 6-7). The exact nature of such algorithms depends upon the approaches devised by the developers. The reader is referred to (Refs. 11-18) which provide insight into the approaches used successfully by leading TGS designers.

### F. Isotopic Composition

In principle, isotopic abundance or composition could be determined on a per voxel basis. In practice, this is not done because of the poor statistical quality of the data. Since it is generally the case that the isotopic composition is uniform throughout the sample a total spectrum consisting of the sum of all emission grabs is analyzed using the isotopic analysis program. Many papers have been written on these techniques and the reader is referred Reference 20, although specific to a particular software package, nevertheless provides a complete set of references and a comprehensive review of the field.

## IV OPERATIONAL CONSIDERATIONS

### A. Calibration Considerations

Initial Mass Calibration

An initial mass calibration must be established before performing measurements. This is done for the principal isotope for the material type involved in the measurement campaign. For example, if measurements are to be done on material type 52, then Pu-239 would be the isotope used for calibration because Pu-239 is the principal isotope for material type 52. A different calibration is required for each primary isotope and calibration standards must be NIST traceable.

Documenting a calibration plan is helpful to address mass calibration factors such as: the mass range for which the calibration will be done, the ranges for which requirements must be met, the number of replicates for each mass range, specific sources to be used, source positions in the drum, matrix drum to be used, collimator settings and count times and layers, as well as a justification for these selections. The range of sources chosen for calibration must be representative of the activity range or gram loadings of the material to be assayed.

Prior to establishing an initial mass calibration, performance checks must be done for detection efficiency, energy calibration, energy resolution and background to insure that the system is operating in a consistent manner. All performance checks must be within established control limits before proceeding with the calibration.

Gamma Ray Spectroscopy System Setup

An Initial Energy Calibration must be performed prior to each measurement campaign and verified each time power to the system has been interrupted. The gain might for example be set to achieve 0.186 keV/channel which for a multi-channel analyzer (MCA) full scale setting of 8192 channels produces an energy range from approximately 0 keV to 1523 keV, depending upon the exact value of the zero offset. The gain value may change depending on the physical

nature of the measurements to be performed but is fixed once the measurement campaign has begun.

The Initial Energy Calibration is established by loading a region of interest (ROI) that includes the 88.036 keV peak of Cd-109 and the 400.65 keV peak of Se-75. The shutter is then opened and spectral data is collected to develop well-formed peaks (approximately 10,000 integral number of counts). As soon as sufficient data is collected, the curser is positioned on the centroid channel (2154±2) for the 400.65 keV peak of Se-75. If the channel number is not within this range, the gain and offset are adjusted until the peak lies within this range. The same is done for the 88.036 keV peak of Cd-109 which should have a centroid channel of 473±2. If the channel number is not within this range, the gain and offset are adjusted until the peak lies within this range.

If the desired gain is 0.186 keV/ch then the slope should always be within this range: 0.185528≤m≤0.186413. The slope and intercept are calculated from the following equations:

$$m = (y_2 - y_1)/(x_2 - x_1)$$

where

$m$ = the slope of the calibration line (keV/Ch)

$y_1$ = the energy of the 88.036 Cd-109 peak

$y_2$ = the energy of the 400.65 Se-75 peak

$x_1$ = the centroid channel number of the 88.036 Cd-109 peak

$x_2$ = the centroid channel number of the 400.65 Se-75 peak

and

$$b = y_1 - m\,x_1$$

where

$b$ = the y intercept of the calibration line (keV)

The y intercept should be within the range: -0.5100 keV ≤b≤0.652502 keV, i.e. the first channel should be within this energy range.

Calibration Confirmation

After the initial mass calibration and after each re-calibration, a calibration confirmation is required to demonstrate that the calibration was established correctly. This is accomplished by performing a series of replicate measurements using a non-interfering matrix. The standards to be used should be different than those used for the initial calibration and must be NIST traceable and span the activity range of use. Prior to performing a calibration confirmation, performance checks must be done for detection efficiency, energy calibration, energy resolution and background to insure that the system is operating in a consistent manner. All performance checks must be within established control limits.

Calibration verification

A calibration verification must be performed when significant changes to the system occur, such as relocation, repair or change in major system components (software or hardware). Standards used for verification must be independent of those used for calibration. Secondary standards can be used for the calibration verification if their performance has been correlated with a calibration standard. The standard is measured three consecutive times in a drum with a non-interfering matrix. The average value is then compared with the known or established value. If the calibration verification indicates that the system's response has significantly changed (exceeding 3 standard deviations), a re-calibration must be performed. Prior to performing a calibration verification, performance checks must be done for detection efficiency, energy calibration, energy resolution and background to insure that the system is operating in a consistent manner. All performance checks must be within established control limits.

## B. Typical Operations Procedure

1. Verify that appropriate radiation postings have been posted in the area and that a safety barrier is available to control/restrict access to the scan table.

2. Verify that the detector is cold and that the liquid nitrogen ($LN_2$) dewar has been filled at least 8 hours prior to use. Keep a log sheet to track $LN_2$ levels and fill at least once a week for a standard size dewer. If the detector runs out of $LN_2$, it must be allowed to warm up at least 24 hours. When re-filling the dewar, allow at least 8 hours of cooling time before high voltage is applied.

3. System start-up:
    a. Turn on electronic equipment such as the computer, monitor, printer, spectroscopy system and oscilloscope.
    b. Adjust high voltage settings to meet detector requirements and turn on high voltage.

4. Daily Safety Checks:
    a. Check the oxygen ($O_2$) concentration in the local work area using an oxygen monitor.
    b. Verify that all emergency stop buttons are working properly (i.e. initiate motion on any axis using manual control, and during motion, press an emergency stop).

The motor controller should stop motion immediately. Repeat this for all emergency stop buttons.

c. Verify that vertical and horizontal limit switches are working properly (i.e. initiate the axes using manual control and verify that each axis moves from one limit to the other and that each axis moves to home).

5. Daily System Checks:
    a. Load Measurement Control drum.
    b. Perform assay.
    c. Analyze assay and verify that all data falls within established control limits.
    d. Unload Measurement Control drum.

If all system checks are within control limits proceed with measurements.

6. Measurements:
    a. Load a waste drum
    b. Perform assay.
    c. Analyze assay data.
    d. Unload waste drum
    e. Repeat steps a - d as needed.

**C. Measurement Control**

Performance checks are done to verify that the system is operating in a consistent manner by checking that performance check data falls within established parameters. These checks are done daily at the beginning of each shift or before acquiring measurement data (including calibration) and include checks for detector efficiency, energy calibration, energy resolution and background. Initial control limits are established as part of the initial set up procedure and are established using acquired data from at least six consecutive runs with a warning limit set at two standard deviations (2-sigma) and an action limit set at 3 standard deviations (3-sigma). If performance checks exceed the warning limit they must be re-done. If the replicate run fails a second time, or if performance checks are outside of the 3-sigma limit, further investigation is required before actual measurements can be done.

Detector efficiency is established with use of a Ba-133 source placed inside an empty drum. A piece of foam may be used to center the Ba-133 in the drum and to insure that the Ba-133 source is placed in the same position (location) each time an efficiency control check is done. Assay results are determined by the TGS number for the 355.99 keV gamma ray line associated with Ba-133 and are used to track system efficiency. The TGS number relates the counting rate to the emission rate, i.e., detection efficiency for a source centered in the drum and at a specific energy.

Generally, an Excel spreadsheet is used to calculate the half-life correction as well as to calculate control limits and generate detector efficiency control charts. Control limits are updated as data

is collected. The mean and standard deviation of the TGS number for the 355.99 keV peak is calculated using the following equations:

$$\bar{y} = \sum_{1}^{n} y_i / n$$

where

$\bar{y}$ = the mean TGS number

$y_i$ = the mean TGS number from the ith measurement

$n$ = the number of observations

and

$$S = \sum_{1}^{n} (y_i - y)/(n-1)$$

where

$S$ = the standard deviation of the TGS number

Energy Calibration

Energy calibration control charts are established using the data from the Ba-133 assay collected for detector efficiency. Using appropriate spectroscopy software such as Maestro, the spectra is checked to insure that the 88.036 keV Cd-109 peak (channel 655) and the 355.99 keV Ba-133 peak (channel 2984) are in the corresponding channels. Warning limits for the energy calibration control chart are +/- 2 channels and action limits are +/- 3 channels. Typically, the centroid channel numbers are recorded by the spectroscopy software where an ROI file report is created for the Cd-109 and Ba-133 lines and read into an Excel spreadsheet which generates the energy calibration control charts.

Resolution Control

Resolution control charts are also established using the data collected from the Ba-133 assay. The full width at half maximum (FWHM) for the 88.036 keV Cd-109 peak and the 355.99 kev Ba-133 peak are also determined and saved by the spectroscopy software into the ROI file and read into an Excel spreadsheet which generates the resolution control charts. Upper Warning Limits (UWL) and Upper Action Limits (UAL) are determined in the Initial Control Limits established by the system managers.

Background

TGS analysis properly accounts for background radiation that falls in the Compton continuum portion of the gamma ray spectrum. However, current techniques do not account for background radiation that falls within the gamma ray peaks to be assayed. Therefore, a region of interest (ROI) for the primary isotope is added to the system check ROI file (in addition to the Cd-109 and Ba-133 lines). During the system check, this ROI is used to determine whether there is background radiation that might affect the analysis of the primary isotope exists. The background control chart tracks the ratio of the net count to the uncertainty in the net counts. In a typical case it is assumed that the background peak is not present if this ratio is <4.65. For 100 counts or more in the peak area this implies that at the 2 sigma level the peak is non-existent. If the ratio is >4.65, then a peak may be present and further investigation is needed.

## V. PERFORMANCE EVALUATION IN BLIND TESTS AND ACTUAL FACILITY MEASUREMENTS

A major selling point of TGS has been its overall versatility and freedom from bias. In this section, we will present a small but representative set of results to help the reader determine if TGS is an approach suited for their application. The first data set is from the Performance Demonstration Program (PDP) comparing TGS to a large number of competing technologies in controlled blind tests. The second and third set of results are from large production runs for classes of materials that are very difficult to assay by any technique other than TGS and validate the time and effort invested to develop the technology.

### A. Performance Demonstration Program (PDP)[21]

"The Performance Demonstration Program (PDP) for NDA consists of a series of tests to evaluate the capability for NDA of Transuranic waste (TRU) throughout the DOE complex. Each test is termed a PDP cycle. These evaluation cycles provide an objective measure of the reliability of measurements obtained from NDA systems used to characterize the radiological constituents of TRU waste."(Ref. 21)

The test results that are given in the following figures are from a series of blind tests of 208-L drums of a known matrix (glass, plastic, sludge, etc) and an unknown distribution and mass of the target isotopes. Radioisotope concentrations for the set of tests were varied over a range expected in actual waste characterization activities. Measurement facilities were required to analyze the simulated waste containers using the same procedures used for normal waste characterization activities. The results are mixed and no single measurement performs better than all others for all situations.

Cycle 1 consists of an empty drum (zero matrix) and an ethafoam drum (non-interfering matrix) using weapons grade plutonium to establish baseline non-destructive waste assay system performance characteristics and to provide a means to access system comparability. The empty drum is also useful for verifying fundamental calibrations and is shown in Figure 1.

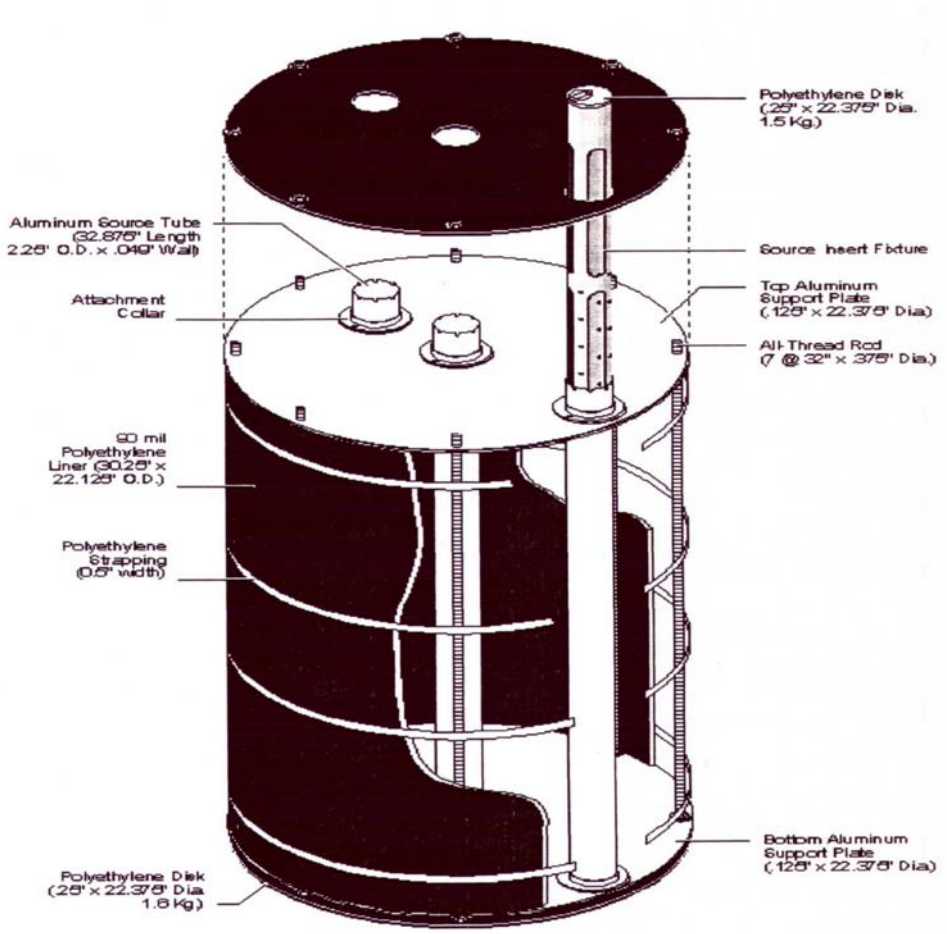


Figure 1: PDP Zero Matrix Drum

Later PDP cycles consist of matrix drums that are used to simulate interfering waste forms and use a variety of isotopes. Manufactured matrix inserts are designed to simulate the physical properties of real waste forms and to test a broad range of measurement interferences that are expected when assaying actual waste. Matrix drums are based on the same general design as the zero matrix drum but simulated waste materials are used to fill the void spaces. Figures 2, 3 and 4 from Reference 21 show a simulated combustible matrix drum, a simulated sludge matrix drum and a simulated metal matrix drum respectively.

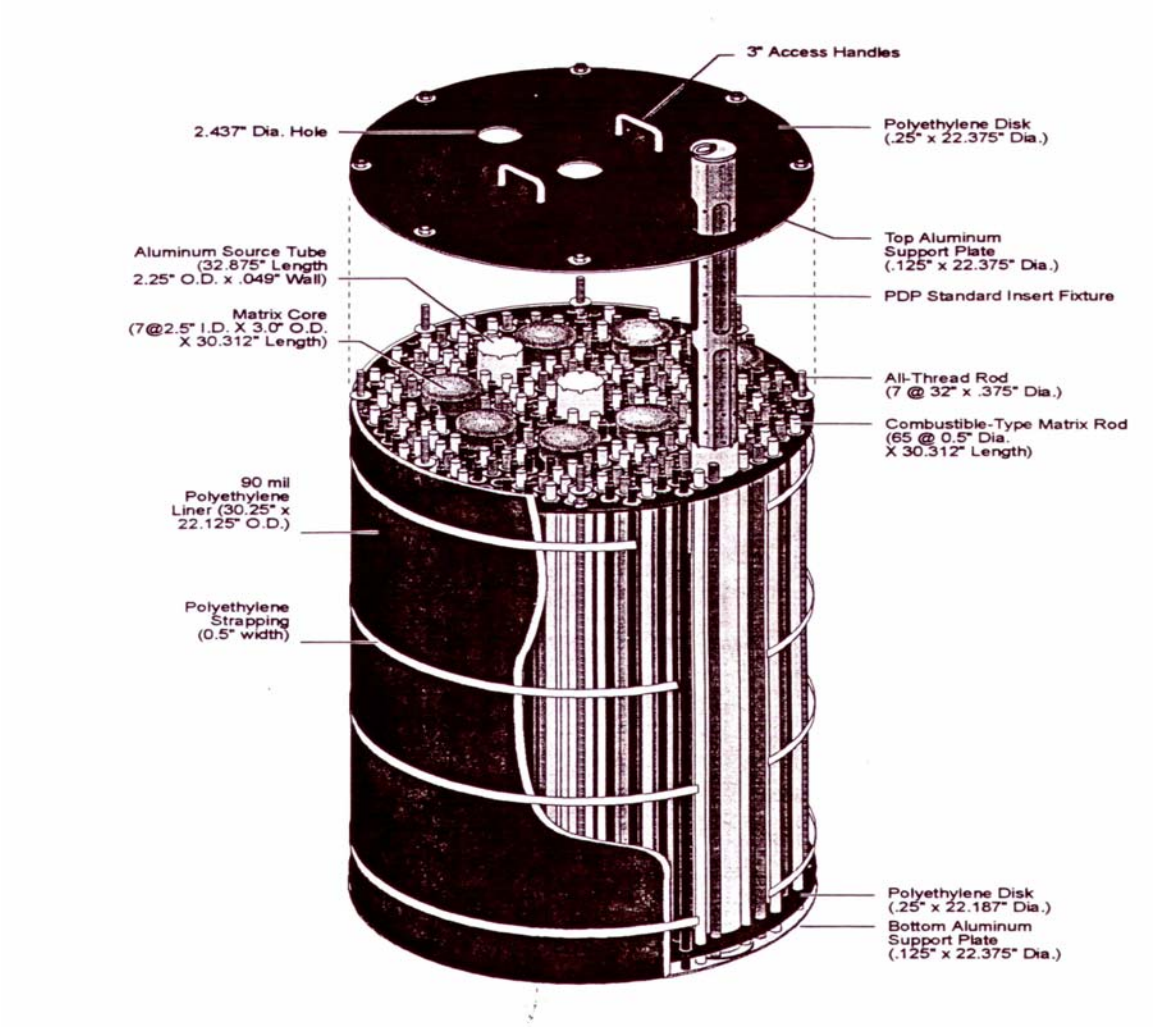


**Figure 2. Assembly configuration of the simulated combustibles matrix drum.**

Note the same source locations as in the empty matrix drum and the intricacy and design detail. The combustible drum has 65 ½" combustible rods to simulate real world loadings. Combustibles are low Z (carbon) and easily measured using gamma methods. The low Z can interfere (moderate and absorb) neutrons thus one expects To see combustibles generally measured with gamma techniques.

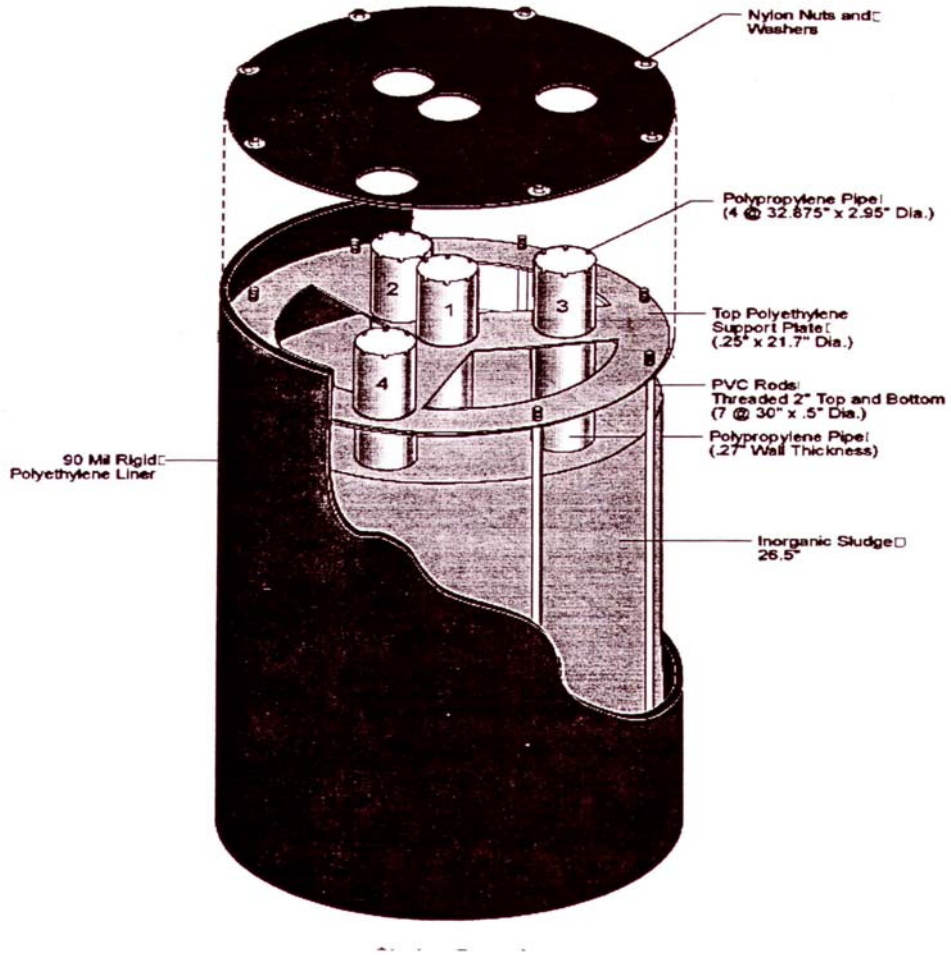


**Figure 3. Assembly configuration of the simulated inorganic sludge matrix drum.**

The sludge drum was difficult for all of the measurement techniques. Generally gamma emissions from materials centered in the drum were effectively shielded and neutrons were highly moderated and absorbed by the matrix. Very few of the initial techniques made it through the sludge test meeting the WIPP WAC. A fourth source tube was added to better identify the measurement limits as a function of source location and matrix attenuation.

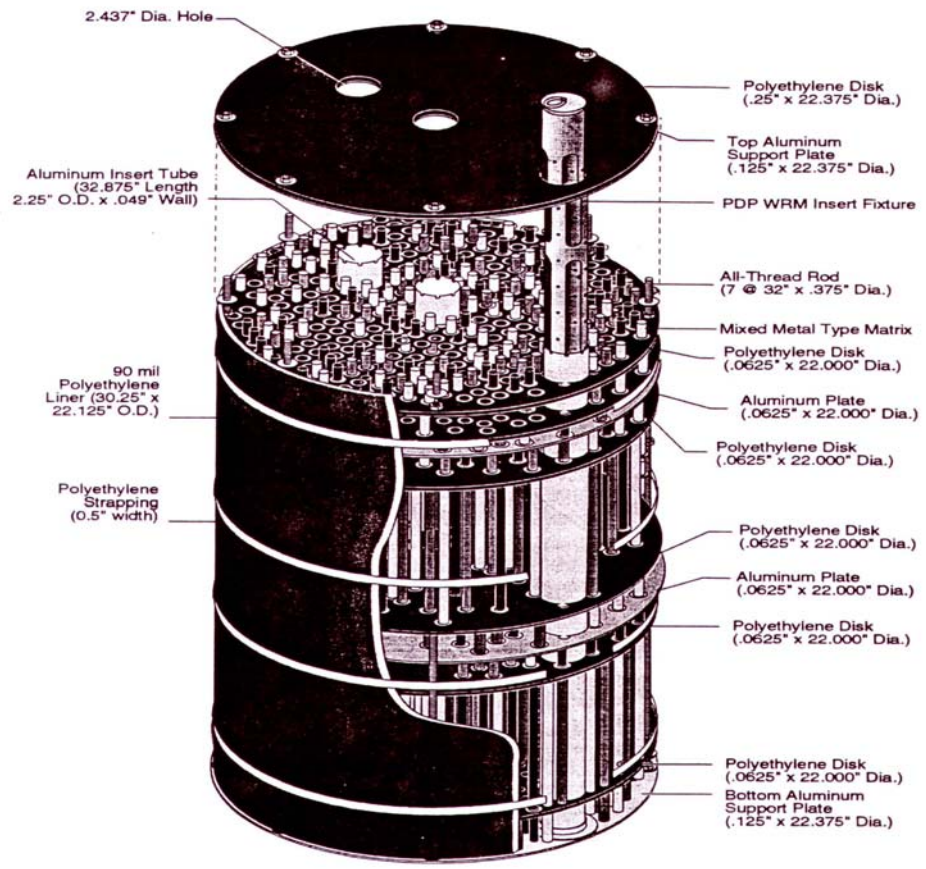


**Figure 4. Assembly configuration of the simulated metals matrix drum.**

The metal drum was the most difficult test of the gamma measurements and generally no more difficult than the empty drum for the neutron measurement techniques. Nevertheless for the low Z metals and density found predominantly in the waste at DOE facilities TGS performs within the WIPP WAC as is found in the actual WIPP PDP tests.

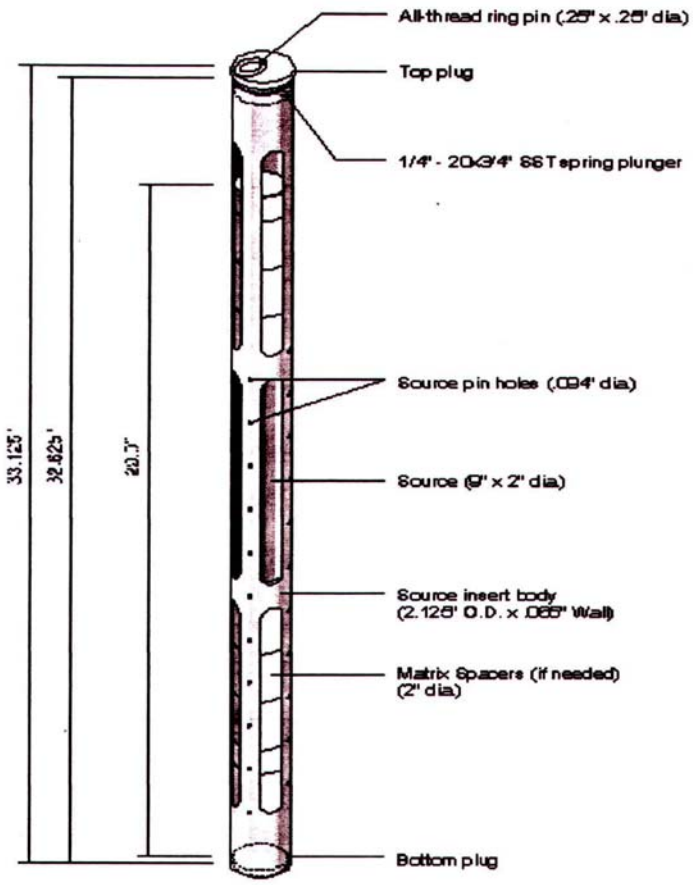


Figure 5: PDP Drum source Insert Fixture

An aluminum source insert fixture (shown in figure 5) allows for the convenient external introduction and precise location of PDP standards within the drum volume. One fixture is provided for each of the insert tube radii on the drum. Standards are placed at a desired vertical location with use of small plunger rods, which are inserted into pin holes on the fixture. The fixture is then placed inside the drum at the appropriate location.

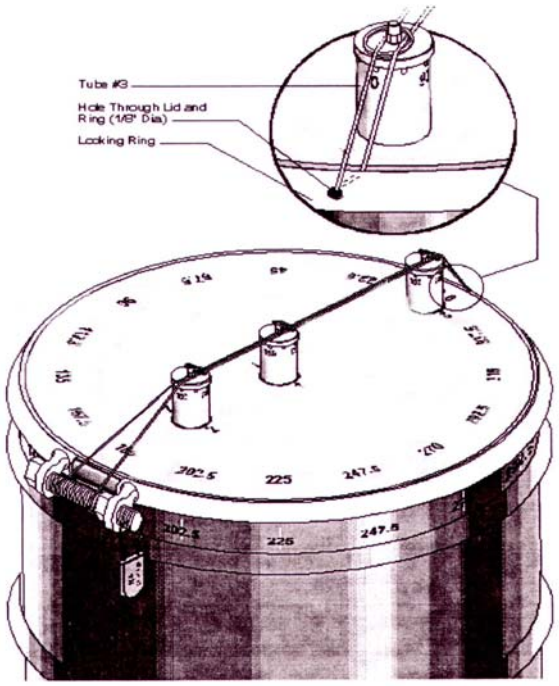


Figure 6: Assembled PDP Drum with TID in Place.

Once the standards are in place, the drum is sealed using an appropriate serialized tamper indicating device (TID). The drum is then transferred to each site's Assay Coordinator for measurement. An assembled PDP drum is shown in Figure 6 from Reference 21.

**Performance Criteria:** Acceptable performance in the NDA PDP tests must be demonstrated by all participating facilities on a semi-annual basis. Single blind samples are prepared twice in each calendar year, approximately every 6 months. The PDP drums must be analyzed using the measurement methods that will be used to analyze WIPP wastes. The facilities and NDA instruments referred to in the results in Fig 10 are as follow:

**Facilities:** INEEL – Idaho National Engineering and Environmental Laboratory, RFETS – Rocky Flats Environmental Technology Site, SRS – Savannah River Site, WRAP – Hanford Waste Receiving and Packaging Facility, LANL – Los Alamos National Laboratory, LLNL – Lawrence Livermore National Laboratory, ORNL – Oak Ridge National Laboratory, PNNL – Pacific Northwest National Laboratory

**Instrument:** HENC – High Efficiency Neutron Counter (passive drum counter), SGS – Segmented Gamma Scanner, PAN – Passive Active Neutron Counter, IPAN – Imaging Passive Active Neutron Counter, TGS – Tomographic Gamma Scanner, CTEN – Combined Thermal

Epithermal Neutron Counter (Active/passive counter), IQ3 – Low-level sensitivity Multi-detector gamma counter, A&PCT – Active and Passive Computed Tomography, APNEA - Active and Passive Neutron Examination and Assay System, PADC - Passive Active Drum Counter, PNCC – Passive Neutron Coincidence Counter, HSNI- High Sensitivity Neutron Instrument

**TGS Performance in the PDP Tests:**

Figure 10 (from Reference 21) summarizes the results of the PDP through 2001 for Cycles 1 through 9. In the comparisons that follow, the TGS results (LANL TGS or RFETS TGS) are results from a skid mounted multi-application development model designed by LANL to support the RFETS closure. On average, the TGS performs as well or better on than any of the instruments and methods in the combustibles and sludge categories. For metals, the passive neutron counters as expected, are the top performers. Nevertheless, for the (low) density and ($Z<27$) atomic number of metals used for the tests the TGS results are well within the WIPP WAC. At higher densities of higher Z metals, TGS will be unable to adequately observe the central regions of the drums and can produce poor results. In the glass category, it appears again that the passive neutron systems are the top performers, although the TGS performance is well within the WIPP WAC requirements.

The category that poses the most difficulty in general for all of the methods is the sludge measurements where TGS clearly is the superior methodology. In all other categories, notwithstanding the caveat regarding metal matrices, TGS is well within the WIPP WAC.

## *Fig. 10. WIPP Performance Demonstration Program Results.*

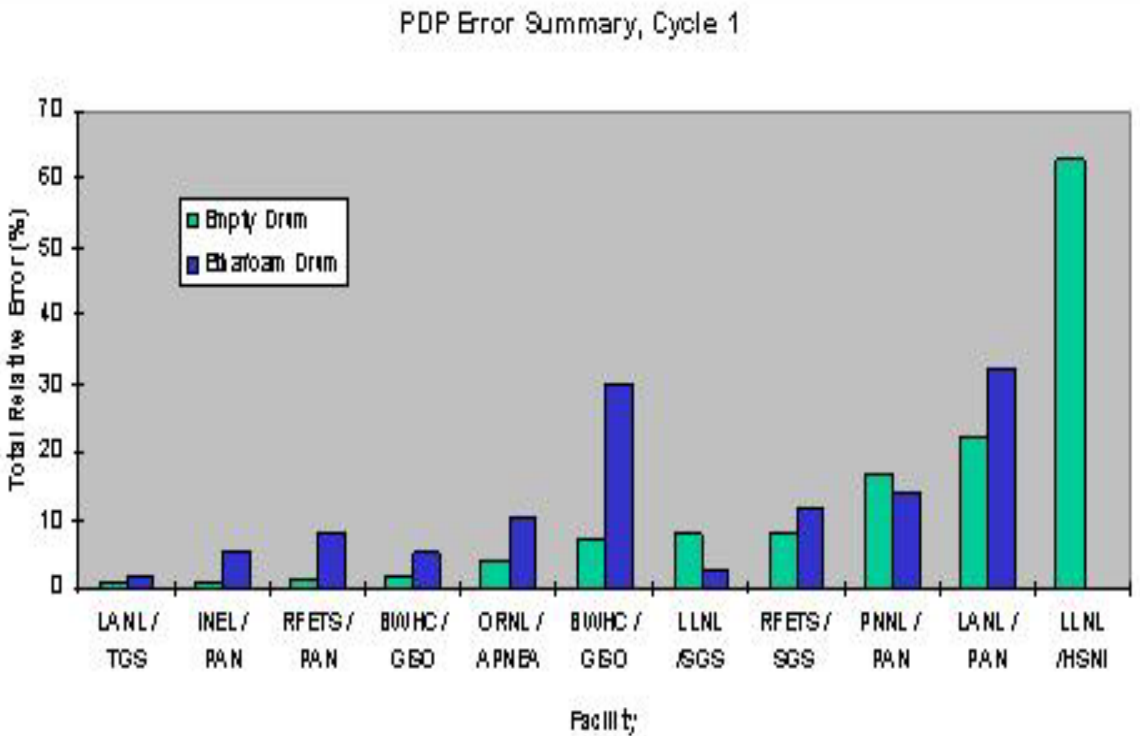

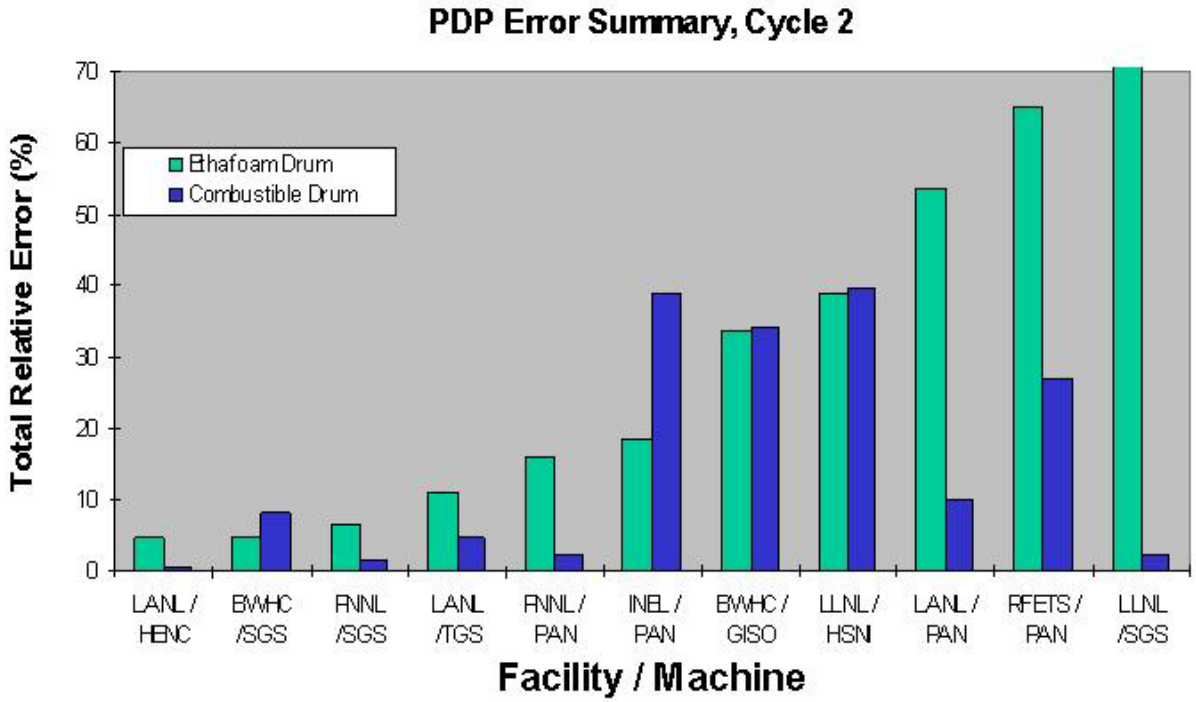
PDP Error Summary, Cycle 2
Total Relative Error (%)
Ethafoam Drum
Combustible Drum
0
10
20
30
40
50
60
70
LANL / HENC
BWHC /SGS
RNNL /SGS
LANL /TGS
RNNL / PAN
INEL / PAN
BWHC / GISO
LLNL / HSN
LANL / PAN
RFETS / PAN
LLNL /SGS
Facility / Machine

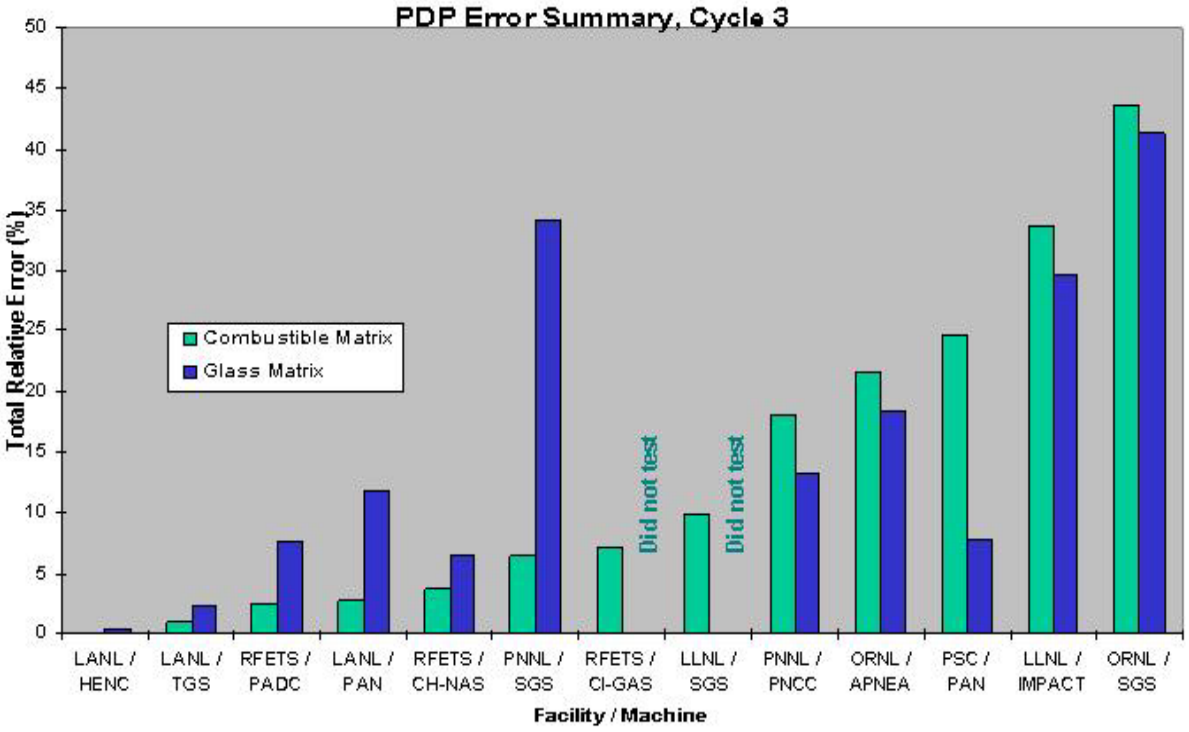
PDP Error Summary, Cycle 3
Total Relative Error (%)
Combustible Matrix
Glass Matrix
Did not test
Did not test
0
5
10
15
20
25
30
35
40
45
50
LANL / HENC
LANL / TGS
RFETS / PADC
LANL / PAN
RFETS / CH-NAS
PNNL / SGS
RFETS / CI-GAS
LLNL / SGS
PNNL / PNCC
ORNL / APNEA
PSC / PAN
LLNL / IMPACT
ORNL / SGS
Facility / Machine

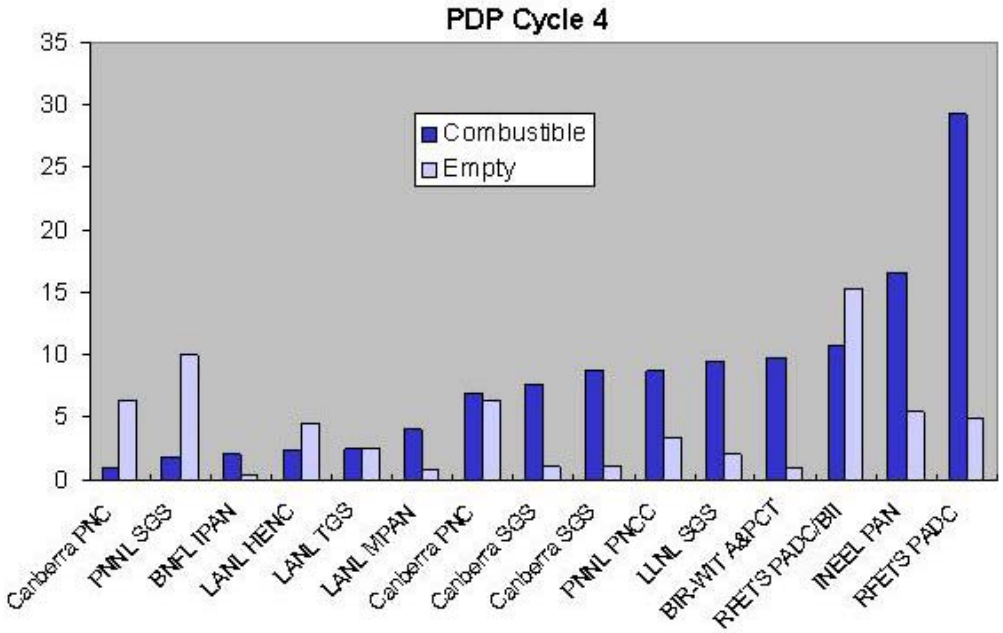


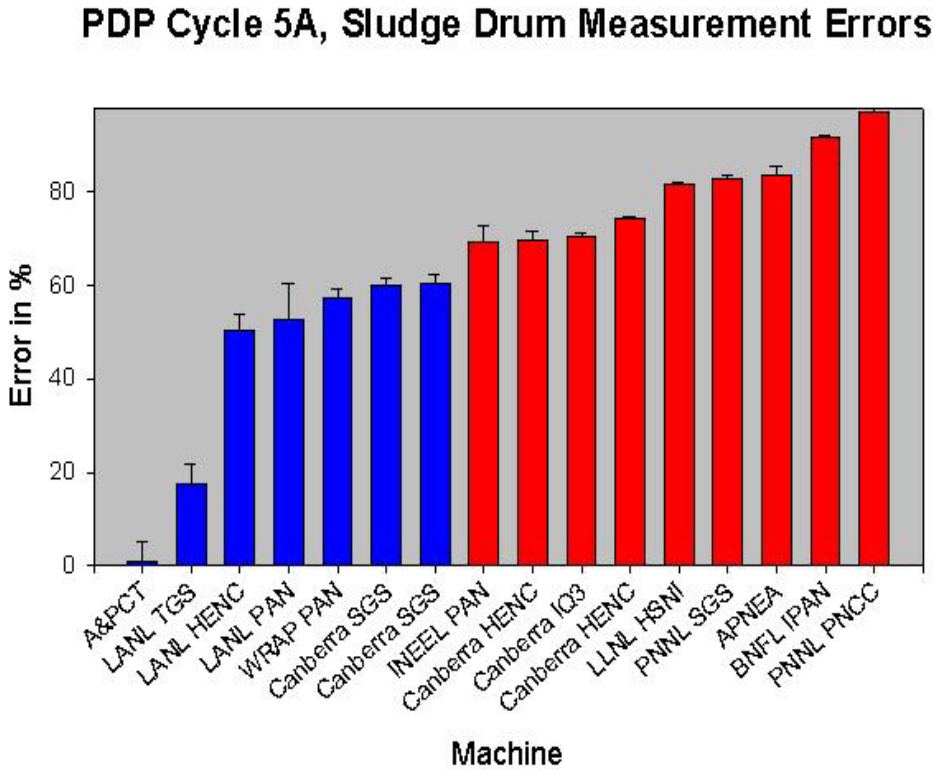


***Fig. 10.*** *PDP results (continued).*

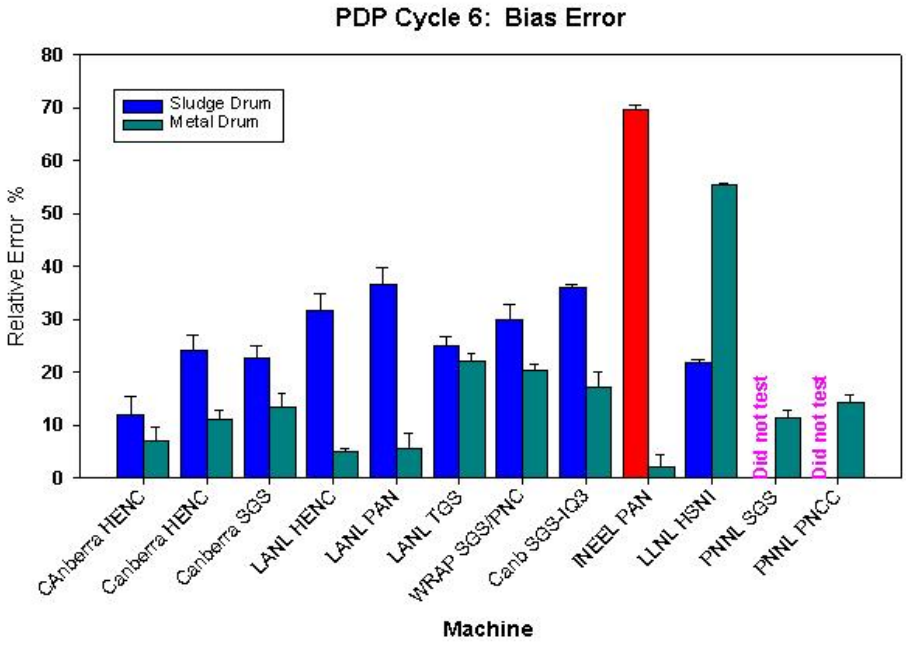


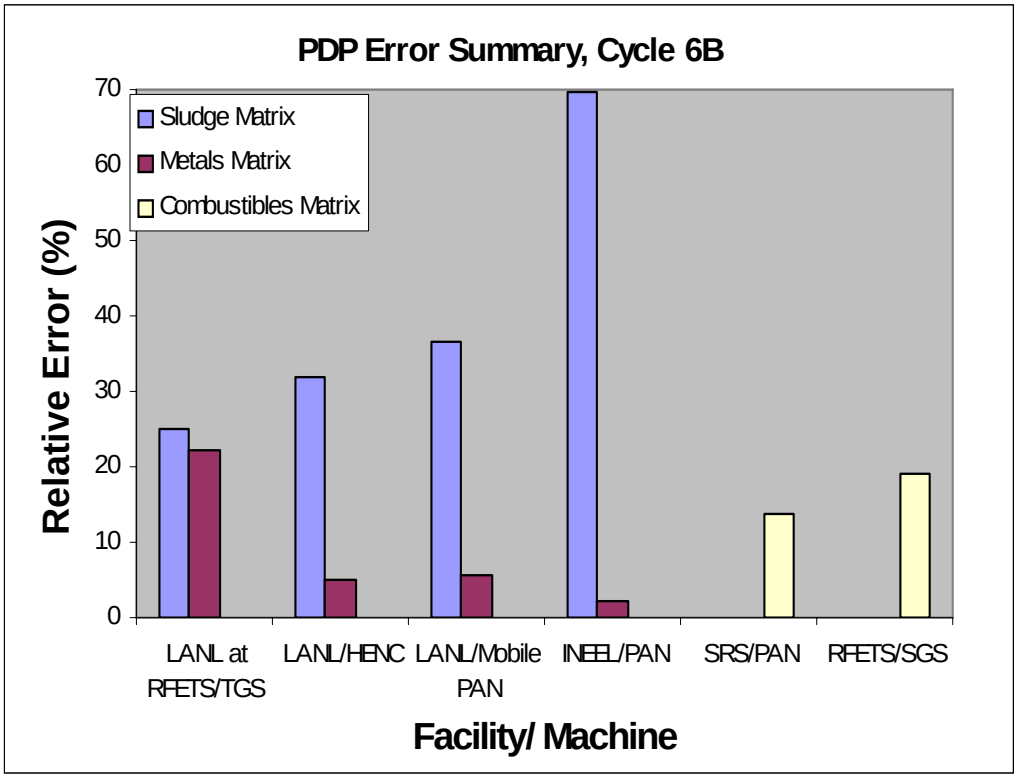


***Fig. 10.*** *PDP results (continued)*

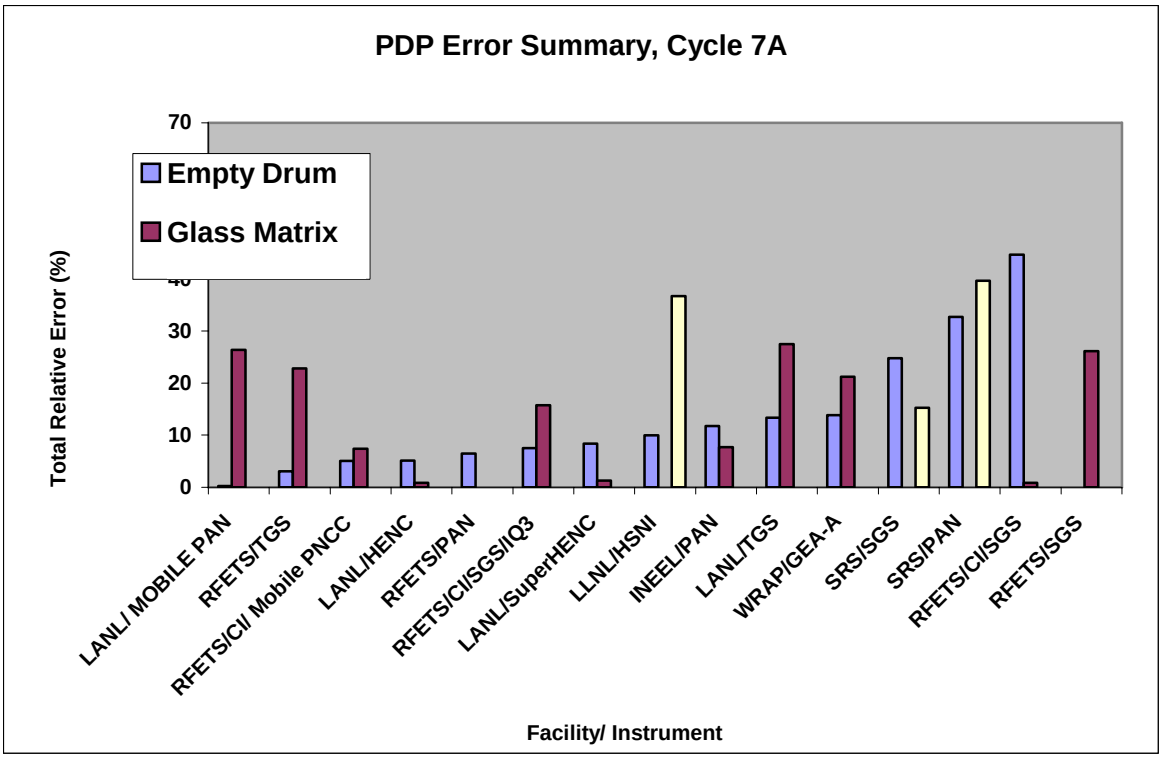


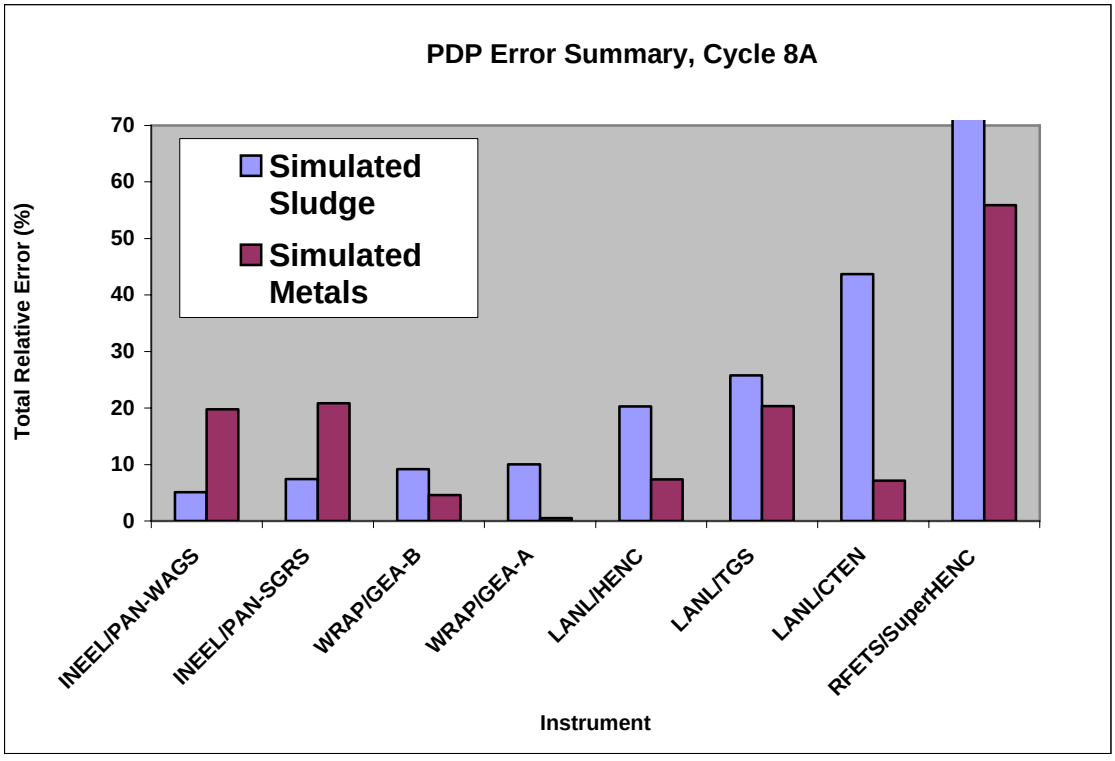


***Fig. 10.*** *PDP results (continued).*

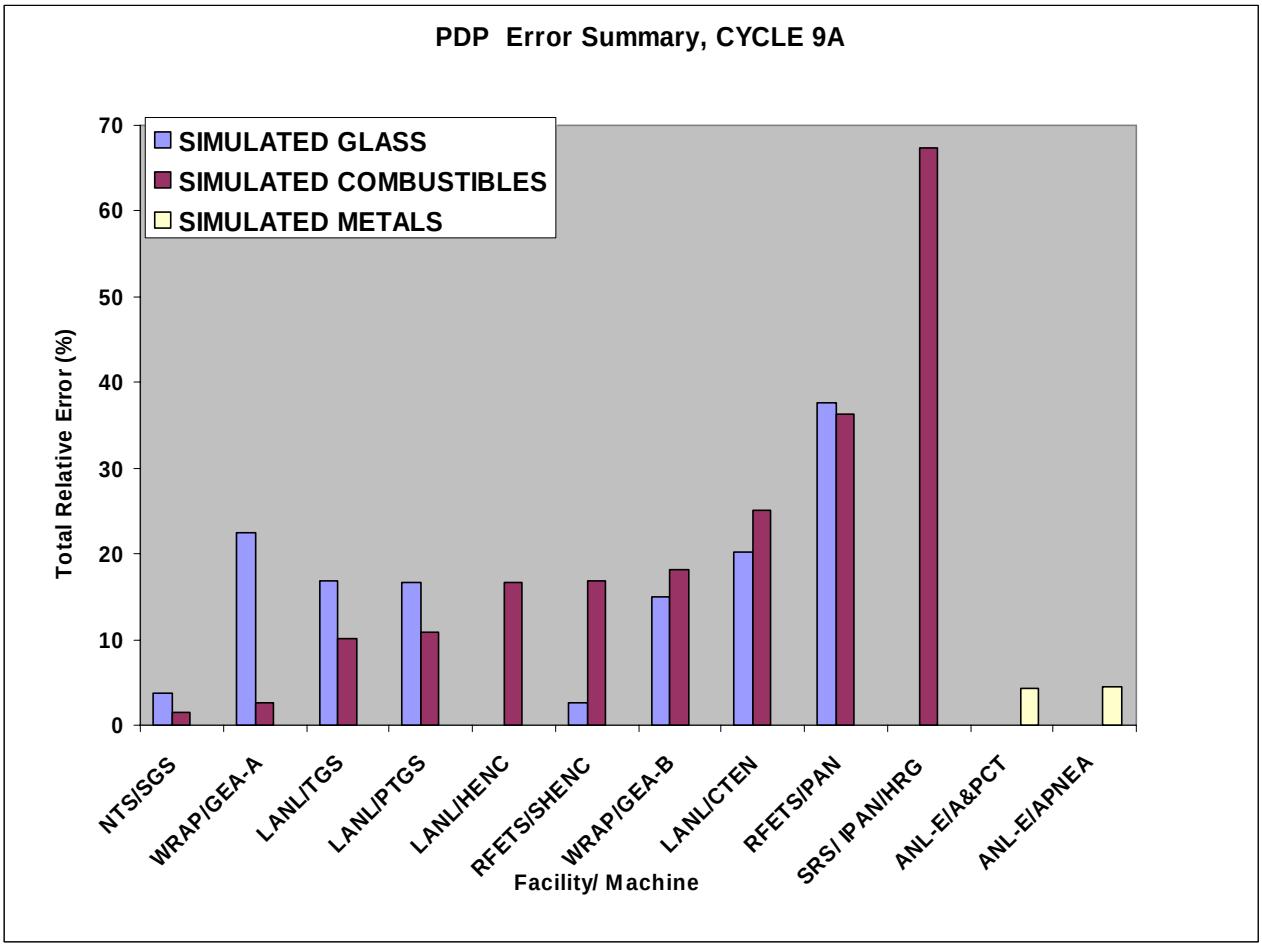


***Fig. 10.*** *PDP results (continued).*

## B. RFETS Pyrochemical Salts[22-25]

The transportable TGS was installed in Building 371 at RFETS for use in the salt repackaging program. Before the start of operations, TGS had demonstrated compliance with safeguards and WIPP requirements (Refs. 22,23). The system was calibrated using SGS standards. To assess the accuracy of the system, assays of electro-refining salts were compared to reference values determined by calorimetry. For each sample, the mass of $^{239}$Pu was determined using TGS with lump corrections. The gamma ray isotopics analysis code FRAM was used to analyze the spectrum acquired by the DSPEC, a commercial multichannel analyzer, using direct signal processing system during the TGS emission scan. The $^{239}$Pu/Pu ratio calculated by FRAM was used with the TGS estimate of $^{239}$Pu mass to determine total Pu. The results of this procedure are compared to the reference values in Table 1. The mean absolute difference between TGS and calorimetric assay was 4.5%. The inventory difference was 2.6% (48 g out of a total of 1839 g). Based on the results of these measurements, TGS was qualified to measure electro-refining salt samples in the 25- to 225-g range and began routine operation.

**Table I**. Comparison between TGS and calorimetric assay of electro-refining salts.

| | Calorimetric Assay | TGS/FRAM | Difference |
|---|---|---|---|
| Sample ID | Total Pu (g) | Total Pu (g) | (%) |
| Z10783 | 45.07 | 44.6 | -1 |
| Z10671 | 142.6 | 151 | 6 |
| Z10668 | 186.6 | 184 | -1 |
| Z10626 | 194.0 | 200 | 3 |
| Z10636 | 151.8 | 160 | 5 |
| Z10637 | 171.7 | 196 | 14 |
| Z10639 | 204.5 | 200 | -2 |
| Z10649 | 162.5 | 161 | -1 |
| Z10731 | 97.26 | 92 | -5 |
| Z10762 | 130.8 | 128 | -2 |
| Z10765 | 121.8 | 131 | 8 |
| Z10781 | 80.63 | 83.2 | 3 |
| Z10782 | 62.36 | 63.6 | 2 |
| Z11395 | 87.43 | 92.5 | 6 |
| Total | 1839 | 1887 | 2.6% |

Pyrochemical salts contain plutonium dissolved in NaCl as well as plutonium in the form of metal shot. These residues also contain high concentrations of $^{241}$Am and other radioactive contaminants. Because the salts are highly inhomogeneous, the established SGS technique, which is based upon homogeneity within segments, could not meet the WIPP criteria for accuracy and bias. Calorimetric techniques are capable of giving reliable results, but throughput is very low requiring an average of 20 hours per package. NDA techniques based upon neutron coincidence counting were unable to provide reliable results because of the inability to establish standards for the wide range of impurities and high $^{241}$Am concentrations that produced a high singles background. As such TGS was developed and applied to the problem materials and the

measurement control results are shown in Figure 17 (from Ref. 22).

The low bias (0.04%) and the high throughput (10 – 20 packages per day) are very notable. The background in the radiation area was significant and demonstrated the advantage of the heavy shielding, described in Section III. Some of the packages were encased in a tin liner, which strongly absorbed the gamma ray emissions and increased the difficulty of the measurements. Below are provided some general guidelines that apply to the measurement of plutonium from Ref. 23 - 25.

Performance results depend both on sample size and material density; the product of these terms is called the areal density [gm/cm$^2$], which is often used to express material "thickness" limitations. As a rule-of-thumb, TGS measurements of $^{239}$Pu using the 414-keV gamma ray generally have better than 10% accuracy for samples with an areal density less than 90 g/cm$^2$ assuming the materials are relatively low atomic number.

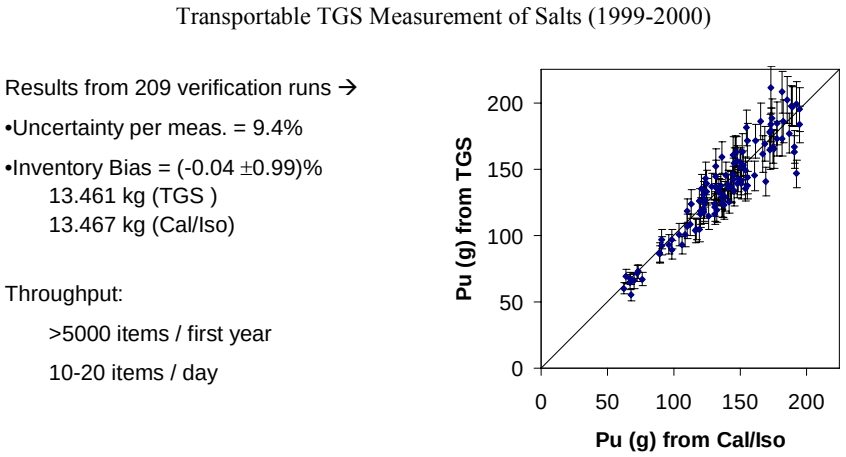


***Fig. 11.*** *Results of electro-refining salts assay at RFETS (Ref. 22).*

For cans approximately 20 cm in diameter, as are typically used for salt repackaging, 10% assays can be achieved at bulk densities of 4.5 g/cm$^3$. TGS is capable of accurately assaying samples that contain regions far exceeding these bulk densities so these estimates tend to be conservative. The precision that can be achieved by TGS varies from sample to sample and depends on the placement of the source, the distribution of attenuating material, collimator parameters, and the mass of SNM present in the sample. As a general rule, 0.5 g $^{239}$Pu in low-density matrices with less than one-hour acquisition time is a mass limit below which measurements become unreliable (Ref. 23). It should be noted that for small homogeneous mass samples (< 5 g), SGS can produce the equivalent precision of TGS with shorter counting times. For example, for a 1-g sample and typical collimator settings, a 20-min SGS scan produces the same precision as a 1-h TGS scan. For samples less than 10 g $^{239}$Pu, precision differences are not a significant issue and the presence of any sample heterogeneity will generally lead to more favorable results using TGS.

## C. Uranium Applications

### 1. RFETS Experience

TGS was primarily developed to assay plutonium in difficult matrices. However, in June 1997, the transportable TGS was deployed in Building 886 at RFETS to assay approximately 200 208-L drums containing waste contaminated with highly enriched uranium, HEU (Ref. 26). In this case, the materials were contaminated with solutions containing uranium and other elements including boron. The boron biased the active neutron measurements and the HEU had too little neutron output for passive measurements. Inhomogeneities ruled out SGS and the very low heat output precluded calorimetry. The materials were primarily contaminated with uranyl-nitrate solutions and consisted of low-Z matrices of borosilicate glass, paper, plastics, cardboard, light metals, soil, and chemical waste all packaged in 208-L drums. The mass of $^{235}U$ ranged from less than 5 g in approximately 80% of the drums to 60 g in a few cases. All of the drums with assay values less than 15 g were shipped offsite for burial. Those with greater assay values were repackaged using the TGS images to facilitate the repackaging. The lower measurement limit was approximately 0.5 g $^{235}U$ for the low-density matrices. This work was important in providing evidence that the TGS technology applies to a wide collection of uranium items that are difficult or impossible to assay by any other means.

### 2. Survey of Excess HEU Materials across the DOE Complex

Because TGS uranium assay is not yet as widely done as TGS plutonium assay, some general information is provided here to assist the reader in assessing the use of TGS for uranium assay. The following tables indicates the amounts of uranium at various sites across the DOE complex (Ref. 27-28).

**Table 2.** Excess HEU at DOE Sites

| Facility | Excess Uranium (Tonnes) |
|---|---|
| Idaho | 23.0 |
| Pantex | 17.0 |
| Portsmouth | 22.0 |
| Oak Ridge | 85.0 |
| Savannah River | 5.0 |
| Total | 174.0 |

**Table 3.** Excess HEU Material Forms at DOE Sites

| Material Form | Excess Uranium (Tonnes) |
|---|---|
| Metal | 87.0 |
| Irradiated fuels/targets | 29.6 |
| Compounds | 17.4 |
| Reactor Fuel | 19.1 |
| Oxide | 15.7 |
| Other | 5.2 |
| Total | 174.0 |

## 3. Relative Comparison of TGS Measurements of HEU and Pu

The safeguards community has gained considerable background in the TGS measurement of plutonium in a variety of matrices. It is not generally recognized that TGS is also well suited for uranium measurements. To facilitate the readers' appreciation for the ability of TGS to handle a large fraction of uranium contaminated materials, a quantitative comparison of the assay expectations is made below between HEU and plutonium for a typical assay geometry (Ref 29). The tables are based on the assay of 208-L drums observed by a 50% efficient Ge detector as is commonly used for TGS. It is assumed that the attenuating material at a thickness equivalent to half the drum diameter and at the specified Z, is sufficient to reduce the 414-keV gamma ray of $^{239}$Pu by a factor of 100. This condition sets a conservative upper limit on the matrix density, corresponding to a factor of $10^4$ reduction in the transmission at 414 keV, which challenges the effective dynamic range of typical Ge detectors. For convenience, the count rate at 414 keV, given this reduction, is taken to be 1 count/sec. Under these same conditions, the identical matrix would reduce the 186 keV gamma ray from $^{235}$U to the count rates given in Table 4a,b. It is important to note that in the absence of any attenuating matrix whatsoever, the count rate per gram would actually be greater for $^{235}$U than for $^{239}$Pu by a factor of approximately 2.5. This results from the higher specific activity of $^{235}$U [4.34 x $10^4$ γ/(s-g) at 185.7 keV] versus $^{239}$Pu [3.42 x $10^4$ γ/(s-g) at 413.7 keV] and the higher intrinsic detector efficiency at 186 keV than at 414 keV (approximately a factor of 2).

The conclusion that one can draw from this comparison is that for conditions conducive to $^{239}$Pu assay, i.e. in matrices that produce an average attenuation of less than a factor of 100 and in matrices that consist of materials such as graphite, combustibles, oxides, fluorides, sludge and ash, the count rate per gram for uranium should be comparable to that of plutonium. It is equally important to realize that when the matrix contains elements with Z greater than 20, the low energy of the principal assay line in uranium (186 keV) strongly limits the application compared to plutonium, which uses the less-attenuated 414-keV line which is less attenuated.

**Table 4a.** Excellent Candidates for TGS Assay

| Isotope | Plastics, Graphite Molds Combustibles, Raschig Rings Z=6 | | Oxides, Fluorides Z=8,9 | | Light Metals Soil, Dirt, Sludge Z=13,14 | | Steel, Iron Z=26 | |
|---|---|---|---|---|---|---|---|---|
| | μ[cm2/gm] | count/s | μ[cm2/gm] | count/s | μ[cm2/gm] | count/s | μ[cm2/gm] | count/s |
| $^{239}$Pu (414 keV) | 0.094 | 1.0 | 0.094 | 1.0 | 0.094 | 1.0 | 0.091 | 1.0 |
| $^{235}$U (186 keV) | 0.125 | 0.55 | 0.125 | 0.55 | 0.127 | 0.50 | 0.145 | 0.16 |
| Counting Ratio (Pu/U) | | 1.8 | | 1.8 | | 2.0 | | 6.3 |

| **Table 4b.** Poor Candidates for TGS Assay | | | | |
|---|---|---|---|---|
| | Medium Z (Tin, Cadmium, Salts) Z=50 | | Heavy Metals Pb, W, U, Pu Z=82 | |
| | μ[cm2/gm] | count/s | μ[cm2/gm] | count/s |
| $^{239}$Pu | 0.105 | 1.0 | 0.203 | 1.0 |
| $^{235}$U | 0.351 | $7x10^{-5}$ | 1.13 | $2.5x10^{-9}$ |
| Counting Ratio (Pu/U) | | $1.4 \times 10^{4}$ | | $4 \times 10^{8}$ |

Owing to this major difference in attenuation as the atomic number of the absorber increases, self-attenuation in uranium presents an especially difficult problem. The next section discusses the problems of lump detection and correction in plutonium and the success that developers have had in inventing techniques for treating the problem to eliminate bias due to self-attenuation. It has been generally recognized by experts that application of the standard plutonium lump detection and correction techniques to uranium does not lead to the same success as in plutonium. In the absence of another technique for lump detection, one must rely entirely on knowledge that the materials are free of lumps to avoid large negative biases. We suggest here an alternative approach for uranium lump detection and correction that may provide the necessary assurance that material with uranium lumps can be easily detected and appropriate corrections applied. The study is in a very preliminary phase, but the relative simplicity of the approach shows sufficient promise to allow those who are contemplating the assay of uranium materials the opportunity to test out the preliminary assumptions.

## VI. Lump Correction Techniques

### A. Plutonium Lump Detection and Correction Technique

An important aspect of minimizing bias in TGS measurements is to identify the presence of small lumps of plutonium and apply suitable corrections for the self-attenuation of the gamma rays from these lumps. The self-attenuation in spherical lumps is formulated in Ref. 30. Even small lumps can cause significant bias, e.g., a plutonium lump of only 2 mm diameter attenuates 70% of the 414-keV gamma rays emitted within it.

An approach to lump detection and correction has been developed and applied successfully for the assay of plutonium-bearing materials (Refs.31 – 33). This approach involves dividing the sample into a homogeneous fraction and a "lumpy" fraction and then estimating the average plutonium lump size using the reduced count rates of lower energy $^{239}$Pu peaks relative to the main 414-keV peak. A convenient means for displaying this technique is shown in Fig. 12. The idea here is to estimate the mass of the plutonium in the sample using each of the high intensity lines of $^{239}$Pu ignoring the effects of self-attenuation. In the presence of lumps, the low energy lines grossly underestimate the plutonium mass and by extrapolation of the mass estimates as a function of gamma-ray energy to 414 keV and beyond a corrected mass is found.

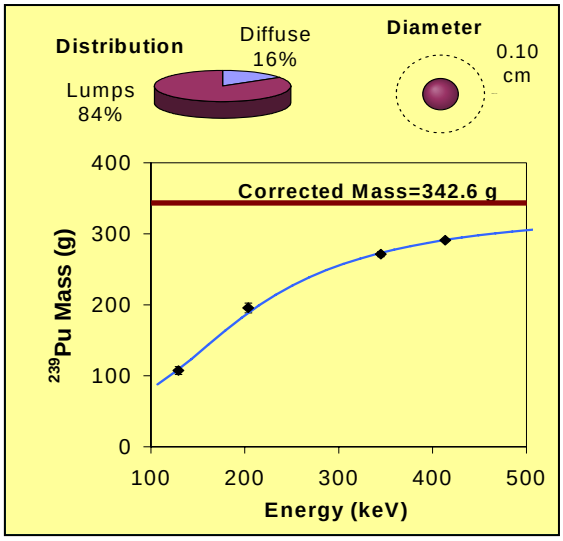


***Fig. 12*** *Lump Correction estimate of the mass of plutonium in a sample*

## B. Standard Pu Lump Correction Doesn't Work for Uranium

The success of this method for $^{239}$Pu derives from the high specific activities of the lower energy gamma rays (in particular those at 129 keV) and the large change in the attenuation coefficient over this energy range. Uranium poses a special problem because the only line of high intensity is relatively low in energy (186 keV) and the other lines are close in energy and have a much smaller range of attenuation coefficients. To acquire a quantitative feel for the problem, it is instructive to compare the gamma rays used for $^{239}$Pu and the corresponding attenuation coefficients in the metal with the corresponding gamma rays of $^{235}$U. Table 5 gives this comparison. The ratio of the attenuation coefficients at 129 keV and 414 keV is 13.8, which compares to a ratio of 1.87 for 143.8 keV and 185.7 keV of uranium. The low intensity of the 205.3-keV and 163.4-keV gamma rays of uranium (factor of 10 less than the 185.7 virtually eliminate them from being useful in a lump correction method as applied above for $^{239}$Pu. Because of these large differences in sensitivity, the Pu technique described above is not feasible for uranium and a new approach has been proposed (Ref 34 ) as is outlined in the following section.

| **Table 5.** Comparing the relative intensity and attenuation coefficients of U and Pu for possible "lump detection gammas." | | | | | |
|---|---|---|---|---|---|
| Plutonium | | | Uranium | | |
| E (keV) | γ/(sec-gm) | μ [$cm^2$.gm] | E (keV) | γ/(sec-gm) | μ [$cm^2$.gm] |
| 129.3 | $1.44 \times 10^5$ | 3.714 | 143.8 | $7.8 \times 10^3$ | 2.737 |
| 203.5 | $1.28 \times 10^4$ | 1.259 | 163.4 | $3.7 \times 10^3$ | 2.003 |
| 345.0 | $1.28 \times 10^4$ | 0.386 | 185.7 | $4.3 \times 10^4$ | 1.463 |
| 413.7 | $3.42 \times 10^4$ | 0.269 | 205.3 | $4.0 \times 10^3$ | 1.333 |

## C. Proposed Technique for Uranium Lump Correction

This technique compares the self-fluorescence of the uranium K X-rays to the thorium K X-rays produced in the decay of $^{235}U$ as shown in Figure 13 from Ref. 34. The upper spectrum comes from a thick uranium metal disk, whereas the lower spectrum comes from two very thin uranium metal disks (~0.03 mm). The $K_{\alpha 1}$ and $K_{\alpha 2}$ x-rays from uranium are at 98.4 and 94.7 keV, respectively. They are the upper two green peaks in the spectra. The corresponding thorium x-rays are at 93.4 and 90.0 keV; they are the lower two green peaks. Note that for the thin foil, where we expect relatively little fluorescence, the ratio of the U x-ray activity to Th x-ray activity is almost one. On the other hand, the same ratio for the thick disk in the upper spectrum, where we expect more fluorescence, is much higher. The thin foil case corresponds to "no lumps" and the thick disk case corresponds to "lumps."

A quantitative comparison, given in Table 6, helps one appreciate the potential sensitivity of this proposed method to correct for "lumps" in uranium measurements.

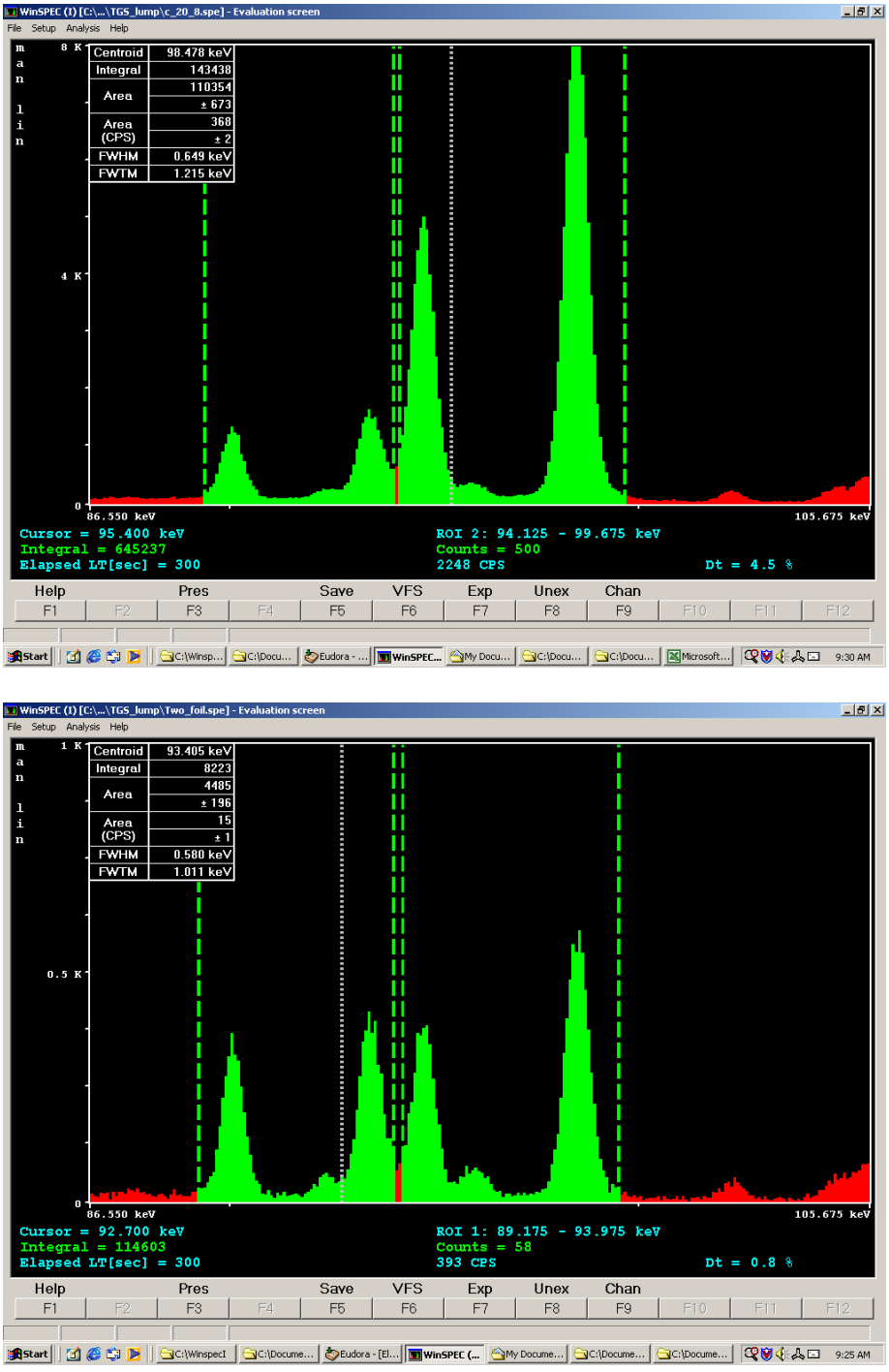


***Fig. 13.*** *Comparison of the fluoresced uranium K x-rays with thorium K x-rays (from U decay) in a thick metal disk (upper spectrum) with those from very thin foils (lower spectrum). The lower energy ROI covers the Th Kα x-rays and the higher energy ROI covers the U Kα x-rays. Note the much higher relative intensity of the uranium x-rays from the metal disk.*

| **Table 6.** Comparison of the peak areas of the fluoresced uranium x-rays in thick versus thin samples of $^{235}U$/ | | |
|---|---|---|
| X Ray Group | Metal Disc | Two Foils |
| Uranium | 110354 | 6141 |
| Thorium | 6141 | 4485 |
| Ratio | 18/1 | 1.4/1 |

The important fact to note in the above table is that a factor exceeding 10 is observed in the ratio for thin versus thick samples, e.g. uranium solutions versus large lumps. This large factor tends to suggest excellent sensitivity to the presence of lumps and with a more careful study even a means of correcting for their presence. As the DOE complex becomes more focused on the uranium assay problem, this technique may become standardized as a means of screening uranium materials suited for TGS assay.

## VI. Commercially Available Systems

With the success of the LANL developed TGS systems at RFETS, the technology was validated and license agreements exist with the following firms:

Antec Corporation
9076 Marshall Court
Westminster, CO 80031

Manufactures drum and can counters in collaboration with Ortec.
BNFL Instruments
4001 Office Court Drive, No. 800
Santa Fe, NM 87505

Has available custom TGS systems for Uranium and Plutonium applications
Ortec
801 South Illinois Ave
Oak Ridge, TN 37830
Distributes TGS systems in collaboration with Antec Corporation.

Figure 14 shows two instruments that are currently available and fielded at several DOE sites. The Model 3800 drum system from Ortec/Antech measures up to 400 liter drums and combines the TGS applications with Pu Isotopics Analysis using the PCFRAM Isotopics Code. Another model similar in function is available for smaller samples.

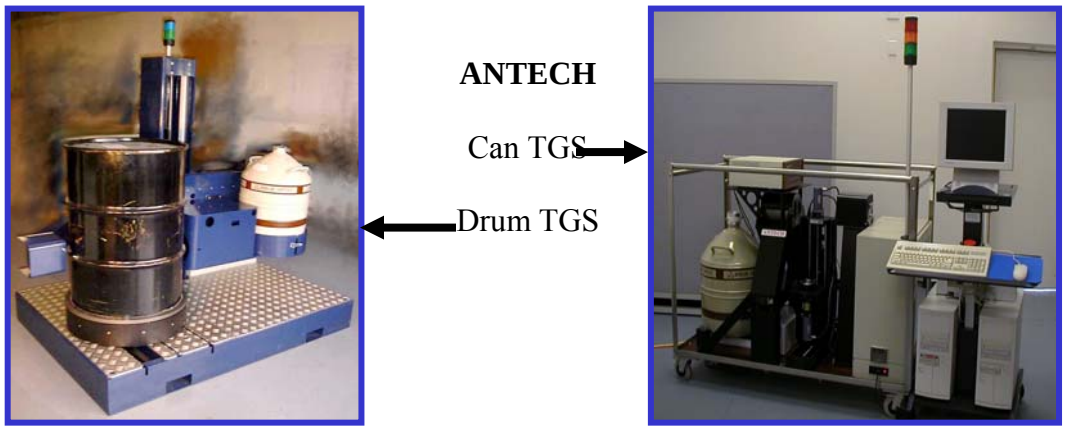


**Fig. 14. Commercially available TGS systems**

## REFERENCES


1. R. J. Estep, "Assay of Heterogeneous Radioactive Wastes by Low-Resolution Tomographic Gamma Scanning," *ANS Transactions* **62**, 178 (1990).

2. S. Kawasaki, et. al, "Radioactivity Measurement of Drum Package Waste by a Computed Tomography Technique" *Applied Radiation and Isotopes* **41,** 983(1990).

3. R. J. Estep, and K. Sherwood, "A Prototype Tomographic Gamma Scanner for Assaying 208-liter drums," Los Alamos National Laboratory report LA-UR-91-61 (1991).

4. H.E. Martz et. al., "Quantitative Waste Assay Using Gamma-Ray Spectrometry and Computed Tomography," Proc. *14th Annual Mtg, Salamanca*, Spain, May 5-8, 1992, European Safeguards Research and Development Association (1992).

5. R. Gordon, "A Tutorial on Algebraic Reconstruction Techniques (ART)" *IEEE Transactions* **NS-21** 78 ff. (1974).

6. R. Gordon, R. Bender, and G. Herman, "Algebraic Reconstruction Techniques (ART) for Three-Dimensional Electron Microscopy and X-ray Photography," *Journal of Theoretical Biology* **36**, 105-117, (1970).

7. G. Hounsfield, "A Method of an Apparatus for Examination of a Body by Radiation Such as X-ray or Gamma Radiation," Patent specification 1283915, The Patent Office, (1972).

8. G.N. Ramanchandran and A.V. Lakshminarayanan, "Three-Dimensional Reconstructions from Radiographs and Electron Micrographs: Application of Convolution Instead of Fourier Transforms," *Proceedings of the National Academy of Sciences*, **68**, 2236 - 2240, (1971).

9. G. Herman and A. Naparstek, "Fast Image Reconstruction Based on a Radon Inversion Formula Appropriate for Rapidly Collected Data," *SIAM Journal of Applied Mathematics* **33**, 511-533, (1976).

10. L. A. Shepp and U. Vardi, "Maximum Likelihood Reconstruction for Emission Tomography," *IEEE Trans. Medical Imaging*, M1-1, 2 (1982)

11. R. J. Estep, "TGS-Fit: Image Reconstruction Software for Quantitative, Low Resolution Tomographic Assays" Los Alamos National Laboratory report LA-12497-MS (1993).

12. R. J. Estep, T. H. Prettyman and G. A. Sheppard, "Tomographic Gamma Scanning to Assay Heterogeneous Radioactive Waste," *Nuc. Sci. Eng*. **118** 145-152, 183-184 (1993).

13. T. H. Prettyman, R. J. Estep, and G. A. Sheppard, "Development of a Tomographic Instrument for Tomographic Nondestructive Assay," *Trans. Am. Nuc. Soc*. **69** 183-184 (1993). Los Alamos National Laboratory report LA-UR-93-2580 (1993).

14. R. J. Estep, "A Preliminary Design Study for Improving Performance in Tomographic Assays," Los Alamos National Laboratory report LA-12727-MS (1994).

15. T. H. Prettyman, R. A. Cole, R. J. Estep, and G. A. Sheppard, "A Maximum Likelihood Algorithm for Gamma-ray Tomographic Nondestructive assay," *Nucl. Instr. Meth*. **A 356,** 470-475 (1995).

16. T. H. Prettyman, "Precision Estimates for Tomographic Nondestructive Assay," *Proceedings of the 5th International Conference on Facility Operations-Safeguards Interface* (American Nuclear Society, Inc., La Grange Park, Illinois 1995), ANS Order No. 700226, pp. 191-199.

17. T. H. Prettyman, L. A. Foster, and R. J. Estep, "Detection and Measurement of Gamma-Ray Self-attenuation in Plutonium Residues," Proceedings of *INMM **37***, 130-136 (1996)

18. T. H. Prettyman, "ARC_TGS User's Manual," Los Alamos National Laboratory Transuranic Waste Characterization/Certification Project – Records Management, TWCP-1493 (1998).

19. J. Radon, "Uber die Bestimmung von Funktionen Durch Ihre Intergralwerte Langsgewisser Mannigfaltigkeiten (On the Determination of Functions from their Integrals Along Certain Manifolds," *Berichte Saechsische Akademie der Wissenschaften*, **29**, pp. 262 - 277, 1917.

20. T. E. Sampson, T. A. Kelley and D. T. Vo "Application Guide to Gamma-Ray Isotopic Analysis Using the FRAM Software," Los Alamos National Laboratory Report LA-14018 (2003)

21. "Performance Demonstration Program Plan for Nondestructive Assay of Drummed Wastes for the TRU Waste Characterization Program," Rev 0.1, U. S. Dept of Energy, Carlsbad Field Office DOE/CBFO-91-1005 (Mar 22, 2001)

22. T. H. Prettyman, S. E. Betts, D. P. Taggart, R. J. Estep, N. J. Nicholas, M. C. Lucas, and R. A. Harlan, "Field experience with a Mobile Tomographic Nondestructive Assay System," Proceedings of the *4th Nondestructive Assay and Nondestructive Examination Waste Characterization Conference*, Salt Lake City, Utah (October 24-26, 1995) 109-137.

23. T. H. Prettyman, S. E. Betts, A. C. Muscatello and D. Catlett, "Final Report on the Mobile TFS Demonstration at Rocky Flats," Los Alamos National Laboratory report LA-UR-98-4052 (1998).

24. David J. Mercer, J. Steven Hansen, John P. Lestone, Thomas H. Prettyman, and Larry Kayler, "TGS Measurements of Pyrochemical Salts at Rocky Flats," *Nucl. Mater. Manage.* **XXX** (Proc. Issue/CD ROM) and Los Alamos National Laboratory report LA-UR-01-3509.

25. D. J. Mercer, T. H. Prettyman, M. E. Abhold and S. E. Betts, "Experimental Validation of Tomographic Gamma Scanning for Small Quantities of Special Nuclear Material," Los Alamos National Laboratory Report LA-UR-97-2804 (1997).

26. D. J. Mercer, S. E. Betts, T. H. Prettyman, C. D. Rael, "Tomographic Gamma Scanning of Uranium Contaminated Waste at Rocky Flats," Los Alamos National Laboratory report LA-UR-98-2922 (1998).

27. "A Strategic Approach to Integrating the Long-Term Management of Nuclear Materials," The Department of Energy's Integrated Nuclear Materials Management Plan, A Report to Congress, June, 2000.

28. "Highly Enriched Uranium, Working Group Report on ES&H Vulnerabilities Associated with the Department's Storage of Highly Enriched Uranium," US DOE, Dec,1996.

29. J. S. Hansen, Unpublished Data (2002)

30. J.-P. Francois, "On the Calculation of the Self-Absorption in Spherical Radioactive Sources," *Nucl. Instr. Methods* **117**, 153-156 (1974).

31. T.H. Prettyman, J. K. Sprinkle and G. A. Sheppard, "A Weighted Least Squares Lump Correction Algorithm for Transmission Corrected Gamma Ray Nondestructive Assay" *Nucl. Mater. Manage*. **XXII**, 682-690 (1993).

32. T.H. Prettyman, J. K. Sprinkle and G. A. Sheppard, "Performance of an Advanced Lump Correction Algorithm for Gamma Ray Assays of Plutonium," Los Alamos National Laboratory report, LA-UR-94-2477 (1994).

33. T. H. Prettyman, L. A. Foster, and R. J. Estep, "Detection and Measurement of Gamma-Ray Self-Attenuation in Plutonium Residues," *Nucl. Mater. Manage*. **XXII**, 130-136 (1996).

34. J. S. Hansen, "Tomographic Gamma Scanning of Uranium, A New Lump Correction Technique," *7th International Conference on Facility Operations – Safeguards Interface*, February 29 – March 5, 2004, Charleston, SC.